

1 **Next generation neural mass and field modelling**

2 Áine Byrne^{1,2,*}, Reuben O'Dea³, Michael Forrester³, James Ross³, Stephen Coombes³

3 1. Center for Neural Science, New York University, New York, NY 10003 USA.

4 2. School of Mathematics and Statistics, University College Dublin, Dublin, Ireland.

5 3. Centre for Mathematical Medicine and Biology, School of Mathematical Sciences,
6 University of Nottingham, Nottingham, NG7 2RD, UK.

7 * Corresponding author: aine.byrne@ucd.ie

8 *Call: 50 Years of Modeling Neural Activity: Celebrating Jack Cowan's Career*

9 **Abstract**

10 The Wilson–Cowan population model of neural activity has greatly influenced our
11 understanding of the mechanisms for the generation of brain rhythms and the emergence
12 of structured brain activity. As well as the many insights that have been obtained from its
13 mathematical analysis, it is now widely used in the computational neuroscience community
14 for building large scale *in silico* brain networks that can incorporate the increasing amount
15 of knowledge from the Human Connectome Project. Here we consider a neural population
16 model in the spirit of that originally developed by Wilson and Cowan, albeit with the added
17 advantage that it can account for the phenomena of event related synchronisation and de-
18 synchronisation. This *derived* mean field model provides a dynamic description for the
19 evolution of synchrony, as measured by the Kuramoto order parameter, in a large
20 population of quadratic integrate-and-fire model neurons. As in the original Wilson–Cowan
21 framework, the population firing rate is at the heart of our new model; however, in a
22 significant departure from the sigmoidal firing rate function approach, the population firing
23 rate is now obtained as a real-valued function of the complex valued population synchrony
24 measure. To highlight the usefulness of this *next generation* Wilson–Cowan style model we
25 deploy it in a number of neurobiological contexts, providing understanding of the changes
26 in power-spectra observed in EEG/MEG neuroimaging studies of motor-cortex during
27 movement, insights into patterns of functional-connectivity observed during rest and their
28 disruption by transcranial magnetic stimulation, and to describe wave propagation across
29 cortex.

30

31 **New & Noteworthy:** Here we review a new type of neural mass model that is derived from
32 an underlying spiking network with synaptic interactions. This *mean field model* gives a
33 macroscopic dynamical description in terms of a population firing rate and the degree of
34 within-population synchrony. We consider applications to understanding beta-rebound
35 observed in neuroimaging studies during movement, the effects of transcranial magnetic
36 stimulation on functional connectivity networks, and large-scale cortical wave propagation.

37 **1 Introduction**

38 To recognise that the neuroscience community is fascinated with the physiological basis of
39 brain rhythms is an understatement. Indeed, the study and exploration of mechanisms that
40 coordinate such rhythms has generated many interesting discoveries in neuroscience,
41 including their strong correlation with cognitive processing, and that synchrony between
42 brain regions may regulate large scale neuronal communication (Fries 2005). A wonderful
43 overview of the ‘Rhythms of the Brain’ can be found in the book, of the same title, by
44 György Buzsáki (2011). Hand in hand with advances in knowledge gained from cellular,
45 systems, and cognitive neuroscience, has come complimentary work from the theoretical
46 neurosciences. After the Hodgkin–Huxley single neuron model, the population model of
47 Wilson–Cowan is perhaps the most well-known (Wilson and Cowan 1972, 1973). Building
48 on earlier work by Beurle (1956), the 1970s model of Wilson and Cowan developed a
49 theory for neural dynamics to describe populations of interacting excitatory and inhibitory
50 neurons with, or without, refractory states. Moreover, they introduced many ideas from
51 dynamical systems to the wider community, highlighting that switching, cycling, and
52 information storage could all be viewed using the framework of attractor dynamics. For a
53 nice historical perspective on the development of their ideas we highly recommend the
54 interview between Jack Cowan and Edward Rosenfeld that can be found in Anderson and
55 Rosenfeld (1998), as well as Destexhe and Sejnowski (2009) that covers some of the many
56 theoretical developments that the Wilson–Cowan model has inspired. Much of the
57 development of Jack Cowan’s work in the 1970s took place in the Cummings Life Science
58 Center at the University of Chicago, building on the activity of Nicholas Rashevsky’s
59 mathematical biophysics group that included Leon Glass, Stewart Kauffman, and Art
60 Winfree¹. Jack Cowan’s work tapped into new mathematical results in catastrophe theory
61 (Cowan and Ermentrout 1978), dynamical systems (Ermentrout and Cowan 1979), and
62 pattern formation (Ermentrout and Cowan 1980), and was promoted to the experimental
63 community at events such as the Gordon Research Conferences on Theoretical Biology and
64 Bioinformatics in 1972 and 1973 (with speakers that include other well-known
65 theoreticians such as Wilfrid Rall, John Rinzel, René Thom and Walter Freeman).

66 The Wilson–Cowan model has now been used in a variety of incarnations: as a single-node
67 description of excitatory-inhibitory population dynamics, as a building block for larger-
68 scale brain network modelling studies, and as the underpinning of spatially-extended
69 models of neural dynamics at the tissue scale. These have provided insights including the
70 understanding of visual hallucinations (Ermentrout and Cowan 1979a; Bressloff et al.
71 2001), binocular rivalry (Wilson, Blake, and Lee 2001), travelling cortical waves (Wilson,
72 Blake, and Lee 2001; Roberts et al. 2019), epilepsy (Shusterman and Troy 2008; Meijer et
73 al. 2015), cognitive dynamics of movement (Erlhagen and Schoner 2002), *phase-amplitude*
74 coupling (Onslow, Jones, and Bogacz 2014), and cortical resonant frequencies (Lea-Carnall

¹ Apparently this was also a great time to play ping-pong on the 9th floor, and many thanks to Bard Ermentrout and John Rinzel for tales of Jack’s scientific and ping-pong exploits. The latter covering the gathering of crowds at conferences to watch Jack play Bob May.

75 et al. 2016) to name but a few. When considering variants of the Wilson–Cowan model this
76 list expands even further to include the interpretation of neuroimaging data (Valdes-Sosa
77 et al. 2009), with the most well-known of these Wilson–Cowan style models being those of
78 Zetterberg, Kristiansson, and Mossberg (1978), Jansen and Rit (1995), and Liley, Cadusch,
79 and Dafilis (2002). Moreover, Wilson–Cowan style neural mass models are a key
80 component of the Virtual Brain project that aims to deliver the first simulation of the
81 human brain based on personalised large-scale connectivity (Sanz-Leon et al. 2015).

82 A core part of the Wilson–Cowan modelling framework is the use of a sigmoid function to
83 determine population firing rates in terms of population activity. Although the use of a
84 sigmoid is now ubiquitous throughout computational neuroscience, in the original Wilson–
85 Cowan model formulation this was assumed to arise via some form of averaging over
86 heterogeneity or noise in networks of simple threshold elements. Thus, although the
87 Wilson–Cowan model can be derived from an underlying microscopic dynamics, this does
88 not come from a biophysically detailed description of a spiking neuron. Nonetheless, in the
89 absence of a general mathematical methodology to develop a statistical neurodynamics
90 from networks of conductance-based Hodgkin-Huxley style neurons with chemical
91 synapses, the Wilson–Cowan model has been a hugely popular *phenomenological* model of
92 cortical dynamics.

93 At the tissue level, the spatially extended Wilson–Cowan model can be conceived of as a
94 (spatially continuous) network of neural masses describing population activity and is often
95 referred to as a *neural field*. There are now a variety of neural field models, distinguished
96 by the type of neural mass model from which they are constructed. All of them adopt a
97 form of non-local spatial interaction to describe anatomical connections and signalling
98 along axonal fibre tracts. However, all modern neural field models of cortical tissue trace
99 their roots back to the seminal work of Wilson and Cowan (1972, 1973), recently reviewed
100 in the book ‘Neural fields: Theory and Applications’ (Coombes et al. 2014), and their
101 mathematical formulation has hardly changed since their original work. Since they describe
102 neural population activity at spatiotemporally coarse-grained scales, they invariably lack
103 important physiological mechanisms known to be fundamental in generating brain
104 rhythms, such as dendritic morphology and nonlinear ionic currents. Nonetheless their
105 basic structure has been shown to provide a mechanistic starting point for understanding
106 whole brain dynamics, and such models form the backbone of many cortical modelling
107 studies.

108 Given the wealth of neuroscience data now accruing through projects such as the Brain
109 Activity Map in the US, seeking to establish a functional connectome of the entire brain,
110 there is now a community-wide need to develop the next generation of neural mass and
111 field models that have a stronger connection to biological reality. This is especially
112 important when one appreciates that many large-scale neuroimaging modalities reflect not
113 only the underlying firing rate of a population of neurons, but also their degree of
114 *synchrony*. A case in point is the well-known phenomenon of event related synchrony/de-
115 synchrony (ERS/ERD), as measured by changes in power at given frequencies in
116 electroencephalogram recordings (Pfurtscheller 1999). The neural dynamics underlying
117 ERD and ERS is most likely a manifestation of a spiking network, with enhanced ERS being
118 linked to an increase in the coherence (synchrony) of spike trains. Thus, in view of their

119 coarse-grained natures, neural mass models in isolation are not natural candidates for
120 modelling ERS/ERD; in fact, one cannot model population synchrony with an isolated
121 traditional neural mass model. However, very recent progress in this area has been made
122 for the case of a globally coupled network of quadratic integrate-and-fire (IF) neurons,
123 making use of the Ott-Antonsen ansatz to derive an exact reduced systems of equations (in
124 the thermodynamic limit) (Byrne, Brookes, and Coombes 2017; Coombes and Byrne 2019).
125 This gives rise to a *neural mass* model with a derived firing rate that is a real function of the
126 complex valued Kuramoto order parameter Z for synchrony and is therefore a marked
127 departure from the sigmoidal firing rate functions used by Wilson and Cowan. The
128 relationship between synchrony and rate f takes the explicit form

$$129 \quad f(Z) = \frac{1}{\pi\tau} \operatorname{Re} \left(\frac{1-Z^*}{1+Z^*} \right), \quad (1)$$

130 where τ is the effective membrane time constant of the neurons and Z^* is the complex
131 conjugate of Z . Here Z is governed by a nonlinear differential equation that couples to the
132 chosen model of the synaptic current. The use of the Kuramoto order parameter in
133 neuroscience is now very prevalent, especially as it relates to the original phase-oscillator
134 network model of Kuramoto (Breakspear, Heitmann, and Daffertshofer 2010). However, its
135 role in neural mass modelling has only recently been realised (Luke, Barreto, and So 2013;
136 Laing 2015; Montbrió, Pazó, and Roxin 2015). The contribution of this paper is to give an
137 introduction to a new class of neural mass and field models that utilize $f(Z) = \frac{1}{\pi\tau} \operatorname{Re} \left(\frac{1-Z^*}{1+Z^*} \right)$,
138 highlighting their benefits to large-scale neuronal
139 population modelling in neuroscience.

140 In §2–**Neural mass model** we give a full description of the dynamics that accounts for the
141 evolution of synchrony within a prototypical next generation neural mass model, and how
142 this couples to the dynamics of a conductance based model of a synapse. Moreover, we give
143 an interpretation of all parameters and state variables within this mean-field model in
144 terms of the underlying spiking network dynamics from which it is derived. This section
145 effectively introduces a single node description of an excitatory-inhibitory population in
146 the spirit of Wilson and Cowan, that can either be studied in response to stimulation, or
147 used as a building block for large-scale brain network modelling studies. Before turning to
148 the latter, we first consider the usefulness of a single node model in generating power
149 spectrograms of the type commonly found in electro- and magneto-encephalography
150 (EEG/MEG) studies of movement. The model is relevant for understanding the differences
151 in ERD/ERS observed between healthy controls and schizophrenia patients, and a simple
152 extension to a two-node model with bi-directional coupling can model the disparities seen
153 between contralateral and ipsilateral hemisphere responses to motor commands. The use
154 of a larger network of such next generation neural masses as an *in silico* testing ground for
155 ideas about the mechanism and control of brain states is explored in §3–**Neural mass**
156 **network model**. As well as using the model to probe the link between structural and
157 functional connectivity, we also explore the response of networks to stimulation (for
158 networks built using human connectome data). We demonstrate that this has major
159 potential for the design of improved transcranial magnetic stimulation protocols. Moving
160 away from parcellated models of the cortex, we turn, in §4–**Neural field model**, to
161 continuum models of cortical surfaces. Here we illustrate how the relevant neural field

162 models, with realistic patterns of structured axonal interactions, can be viewed in terms of
163 a generalised brain-wave equation of Nunez type (Nunez 1974). Numerical simulations are
164 used to illustrate the patterns of propagating waves that can be supported, both with and
165 without a form of adaptation that mimics local metabolic processes. Finally, in §5–
166 **Discussion** we discuss the future steps for the development and further application of next
167 generation neural mass and field models.

168 **2 Neural mass model**

169 Neural mass models generate brain rhythms using the notion of population firing rates,
170 aiming to side-step the need for large scale simulations of more realistic networks of
171 spiking neurons. Although they are not derived from detailed conductance-based models
172 they can be motivated by a number of phenomenological arguments (Coombes et al. 2014),
173 and typically take the form of systems of nonlinear ordinary differential equations (ODEs).
174 The Wilson–Cowan neural mass model describes the dynamics of two interacting
175 populations of neurons, one of which is excitatory and the other inhibitory. Interactions
176 between the populations are mediated by a nonlinear sigmoidal firing rate function. In its
177 most simple incarnation, it consists of two nonlinear ODEs, and as such, has been widely
178 studied using techniques from phase-plane analysis and numerical bifurcation theory.
179 Caricaturing the sigmoid with a piecewise linear function also allows for a more explicit
180 mathematical analysis, including the construction of oscillations and the determination of
181 their stability (Coombes et al. 2018).

182 Building on work by Luke, Barreto and So (2013), Laing (2015), and Montbrió, Pazó and
183 Roxin (2015), recent studies at the intersection of theoretical neuroscience and self-
184 organised systems have led to the formation of a generalised neural mass model (Byrne,
185 Brookes, and Coombes 2017; Coombes and Byrne 2019). The model takes a similar form to
186 that proposed by Wilson and Cowan in 1972, and for clarity of exposition we first write the
187 model for a population of neurons with global self-feedback through a set of synapses with
188 overall conductance g . This conductance evolves according to the dynamical system

189
$$Qg = \kappa f(Z), \quad (2)$$

190 with the firing rate $f(Z)$ given by $f(Z) = \frac{1}{\pi\tau} \operatorname{Re} \left(\frac{1-Z^*}{1+Z^*} \right)$, (1).

191 Here κ is the strength of coupling and the differential operator Q is chosen to best capture
192 the temporal characteristics of synaptic response. For the popular α -function synapse, with
193 shape $\alpha^2 t e^{-\alpha t}$ following the arrival of an action-potential at time $t = 0$, we would choose

194
$$Q = \left(1 + \frac{1}{\alpha} \frac{d}{dt} \right)^2, \quad (3)$$

195 and see Byrne, Brookes and Coombes (2017) for other choices. The form of equation
196 $Qg = \kappa f(Z)$, (2) is common in neural mass modelling,
197 albeit with a different form of closure, whereby $Qg = \kappa f(g)$, with f chosen to be a
198 sigmoidal function. The major modelling departure in the use of equation $Qg = \kappa f(Z)$,
199 (2) is that here f is a *derived* quantity and, additionally,

200 it is a function of the dynamic synchrony variable Z , with magnitude R and phase Ψ , so that
 201 $Z = Re^{i\Psi}$. Hence, we have a direct link between the within-population synchrony and the
 202 synaptic activity. The synchrony variable, known as the Kuramoto order parameter evolves
 203 as follows:

$$204 \quad \tau \frac{d}{dt} Z = \mathcal{F}(Z; \eta_0, \Delta) + \mathcal{G}(Z, g; v_{\text{syn}}), \quad (4)$$

205 where

$$206 \quad \mathcal{F}(Z; \eta_0, \Delta) = -i \frac{(Z-1)^2}{2} + \frac{(Z+1)^2}{2} [-\Delta + i\eta_0] \quad (5)$$

$$207 \quad \mathcal{G}(Z, g; v_{\text{syn}}) = i \frac{(Z+1)^2}{2} v_{\text{syn}} g - \frac{(Z^2-1)}{2} g. \quad (6)$$

208 To interpret the model parameters Δ , η_0 and v_{syn} , we must examine the underlying spiking
 209 model from which it is derived, namely the quadratic integrate-and-fire (QIF) network
 210 model. A QIF neuron in a globally coupled synaptic network indexed by $i = 1, \dots, N$ evolves
 211 according to

$$212 \quad \tau \frac{d}{dt} v_i = \eta_i + v_i^2 + g(v_{\text{syn}} - v_i), \quad Qg = \frac{\kappa}{N} \sum_{j=1}^N \sum_{m \in Z} \delta(t - T_j^m), \quad (7)$$

213 subject to *reset* $v_i \rightarrow -\infty$ whenever v_i reaches $+\infty$ in finite time and *fires*. These firing
 214 events occur at times T_i^m , where m indexes the m th time that neuron i fires. The
 215 background drives η_i are chosen from a normalised Lorentzian distribution with centre η_0
 216 and width Δ , and v_{syn} corresponds to the synaptic reversal potential of the neurons. Here,
 217 the inputs η_i are “quenched”, though it is also possible to obtain similar model behaviour
 218 (to that reported below) with identical neurons ($\eta_i = \eta_0$ for all i) driven by noise
 219 (Montbrió, Pazó, and Roxin 2015). For a full description of how to derive $Qg = \kappa f(Z)$,

$$220 \quad (2) \text{ and } \tau \frac{d}{dt} Z = \mathcal{F}(Z; \eta_0, \Delta) + \mathcal{G}(Z, g; v_{\text{syn}}),$$

$$221 \quad (4) \text{ from } \tau \frac{d}{dt} v_i = \eta_i + v_i^2 + g(v_{\text{syn}} - v_i), \quad Qg = \frac{\kappa}{N} \sum_{j=1}^N \sum_{m \in Z} \delta(t - T_j^m),$$

222 (7) as $N \rightarrow \infty$ see Byrne, Brookes, and Coombes (2017) and Coombes and Byrne
 223 (2019). Thus, the mean-field description of a globally coupled QIF network with a shunted
 224 synaptic current modelled using an α -function conductance change is given by just four
 225 ODEs. Two of these, given by $\tau \frac{d}{dt} Z = \mathcal{F}(Z; \eta_0, \Delta) + \mathcal{G}(Z, g; v_{\text{syn}})$,

226 (4), describe the evolution of the complex Kuramoto order parameter for synchrony,
 227 and the other two, given by $Qg = \kappa f(Z)$, (2), describe
 228 how this couples to the dynamics of the synaptic conductance. For simplicity we now set
 229 $\tau = 1$ throughout the rest of this paper (unless otherwise stated). Figure 1 demonstrates
 230 that the dynamics of the order parameter Z and synaptic conductance g for a simulation of
 231 500 QIF neurons described by $\tau \frac{d}{dt} v_i = \eta_i + v_i^2 + g(v_{\text{syn}} - v_i)$, $Qg = \frac{\kappa}{N} \sum_{j=1}^N \sum_{m \in Z} \delta(t -$
 232 $T_j^m)$, (7) (red) and the mean field model, given by $Qg = \kappa f(Z)$,

$$233 \quad (2) \text{ and } \tau \frac{d}{dt} Z = \mathcal{F}(Z; \eta_0, \Delta) + \mathcal{G}(Z, g; v_{\text{syn}}), \quad (4)$$

234 (blue), are closely matched. It is very straightforward to extend the above to treat
 235 populations of interacting excitatory and inhibitory neurons. In this case each neuronal

population has two types of synaptic conductances associated with it, one to describe inhibition and the other for excitation. If each synapse has a conductance change modelled as an α -function then eight first order ODEs are needed to model the four populations of synapses, with a further four required to model the degree of synchrony in the excitatory and inhibitory neuronal populations respectively. This gives a minimal model of a patch of cortex in terms of twelve first-order ODEs, which can be reduced in number by dropping cross-interactions (such as self-inhibition), and/or choosing a first order differential operator for Q , such as $(1 + \alpha^{-1}d/dt)$, describing a *fast* synapse with an exponential decay rate α^{-1} . The form of this minimal model of cortex as a *single* node, encapsulating local interactions of both excitatory and inhibitory type, is generalised from $Qg = \kappa f(Z)$,

$$(2) \text{ and } \tau \frac{d}{dt} Z = \mathcal{F}(Z; \eta_0, \Delta) + \mathcal{G}(Z, g; v_{\text{syn}}),$$

(4) as

$$248 \quad Q_{ab}g_{ab} = \kappa_{ab}f(Z_b), \quad \tau_a \frac{d}{dt} Z_a = \mathcal{F}_a(Z_a; \eta_0^a, \Delta^a) + \sum_b \mathcal{G}(Z_a, g_{ab}; v_{\text{syn}}^{ab}), \quad (8)$$

where $a, b \in \{E, I\}$ represent labels for excitation (E) and inhibition (I), Q_{ab} is obtained from $Q = \left(1 + \frac{1}{\alpha} \frac{d}{dt}\right)^2$, (3) under the replacement $\alpha \rightarrow \alpha_{ab}$ (so that the time course of synaptic responses can differ), and v_{syn}^{ab} is the reversal potential mediating the current from population a to population b .

Neural oscillations, as observed using EEG/MEG, are thought to be the result of neurons synchronising their firing times to create coherent high amplitude oscillations. To better understand these oscillations and how certain tasks can modulate their amplitude, it is important to examine the synchronisation properties of the underlying neurons. Next we discuss how the model can be used to explore ERD/ERS and other changes in neural synchrony.

2.1 Beta rebound

Neural activity in the beta-band (13–30 Hz) has long been associated with movement. In particular, execution of a movement results in a decrease of beta power in the motor cortex, termed movement-related beta decrease, (MRBD), followed by an increase above baseline upon movement termination (post-movement beta rebound; PMBR) (Figure 2(a)). It is hypothesised that this event-related modulation corresponds to changes of synchrony within motor cortex (Stancák and Pfurtscheller 1995). Given that the neural mass model described above can track within-population synchronisation (and that standard neural mass models cannot), it was deemed an ideal candidate for modelling this phenomena by Byrne, Brookes, and Coombes (2017). Simulating a single inhibitory population with a time dependent drive $Qg = \kappa f(Z)$,

$\mathcal{F}(Z; \eta_0, \Delta) + \mathcal{G}(Z, g; v_{\text{syn}})$, (4), the authors linked changes in synaptic activity to changes in the underlying synchronisation (Figure 2(c) & (d)). In the absence of drive the model oscillated at ~ 15 Hz. When the drive was switched on (movement initiation), the beta-band oscillations disappeared. After the drive was

removed (movement termination), the spectral power in the beta-band rebounded above baseline, before it settled back to its original value (Figure 2(d)). Examining the phase plane of the order parameter Z (Figure 2(c)), they showed that after the drive is switched off (green curve) the order parameter is attracted to the edge of the unit disc (maximal synchrony $R = 1$) before spiralling back to the original limit cycle.

Human MEG studies reveal beta rebound on both sides of the motor cortex during movement. The strongest rebound is seen in the contralateral hemisphere, with a weaker rebound in the ipsilateral hemisphere. Contralateral refers to the side of the brain that sends and receives the motor commands, while the ipsilateral hemisphere receives the input indirectly from the contralateral hemisphere, through bi-lateral coupling. In the above we considered a single node, assumed to represent the contralateral motor cortex. To examine the interplay of the contralateral and ipsilateral hemispheres, we introduce a second identical node. The coupling between the two is bi-directional, with a long synaptic timescale. This two hemisphere model successfully produces MRBD and PMBR in both populations with a larger PMBR in the contralateral (driven) hemisphere (Figure 3(a)) than the ipsilateral hemisphere (Figure 3 (b)).

The presence of the second population leads to the emergence of co-existing oscillatory solutions, i.e. different initial conditions can lead to different behaviours. Depending on which of the two states the system is in, it will react differently to the motor command. The magnitude and length of PMBR is also heavily dependent on the phase of the oscillation when the drive is applied (Figure 3(a)-(h)), as well as the oscillatory state it is in. This variability in the model response is akin to MEG recordings, where individual trials show large variability in the magnitude and length of PMBR. It is only upon averaging over many trials that we see the stereotypical MRBD and PMBR, as shown Figure 2(a).

Beta decrease (MRBD) and rebound (PMBR) are special cases of ERD and ERS, respectively. Event-related changes in synchrony are observed in many different brain areas for a range of different frequencies. By modifying the model parameters, we can change the frequency of oscillation of the population and explore other types of ERS/ERD, such as the attenuation of the alpha rhythm upon eye opening. We emphasise again that standard neural mass models, based on Wilson–Cowan style descriptions, cannot describe ERD/ERS because their level of coarse-graining does not allow one to interrogate the degree of within-population synchrony.

2.2 Beta burst

Recent experimental evidence suggests that beta-band activity is stochastically transient, rather than steady and sustained as previously thought (Feingold et al. 2015; Lundqvist et al. 2016). Electrophysiological recordings, such as EEG and MEG, are typically trial averaged to produce clear time-frequency spectrograms. Transiently occurring bursts of beta activity could present as a sustained rhythm in a trial averaged regime, leading experimentalists to search for these *beta bursts* in single trial EEG and MEG data. At a single-trial level, spontaneous brain activity in motor areas indeed shows transient bursts of beta-band activity lasting ~ 150 ms (Sherman et al. 2016). When trial-averaged, this same activity appears sustained with a relatively constant power level.

317 As well as sustained beta oscillations, the model can also support beta bursts when pink
318 noise is added to the system. Using an excitatory-inhibitory pair and setting the parameter
319 values close to the boundary between oscillatory and stationary behaviour, noise can
320 perturb the system temporarily into the oscillatory state. When the system is perturbed
321 into the oscillatory state, we see bursts of high amplitude activity, lasting \sim 200 ms (Figure
322 4(a)). The bursts seen in single simulations occur every few seconds, but when averaged
323 over multiple simulations there is a constant power at roughly 20 Hz consistent with trial
324 averaged data (Figure 4(b)). Interestingly, the time scale of the noise changes the
325 occurrence of the bursts. If the noise frequency is above alpha-band (8 Hz), there is no
326 effect, but for frequencies lower than \sim 8 Hz the number of bursts decreases with noise
327 frequency. Should beta bursts in electrophysiological recordings be characterised by
328 frequency of occurrence in various situations, this model could be used to explore the types
329 of noise responsible for the bursts.

330 **2.3 Neurological disorders**

331 Given the prevalence of EEG/MEG in neuroscience, researchers have begun to ask if these
332 recordings could provide biomarkers for neurological disorders (Lopes da Silva 2013).
333 Abnormal beta oscillations were recently identified as a biomarker of a number of
334 neurological disorders, such as schizophrenia and Parkinson's disease. Among these
335 abnormalities is a reduction in magnitude of beta rebound. Schizophrenia patients show a
336 similar MRBD, but a reduced PMBR when compared to healthy controls (Figure 2(a)-(b)),
337 and the severity of the reduction in PMBR is directly correlated to severity of the disease
338 (Robson et al. 2016). Byrne, Coombes and Liddle (2019) recently demonstrated that this
339 result could be reproduced using the next generation neural mass model described above
340 with a longer synaptic timescale for the glutamatergic receptor responsible for processing
341 the motor input. This result reaffirms the belief that schizophrenia is an information
342 processing disorder, demonstrating that reducing the synaptic transmission rate reduces
343 the magnitude of PMBR.

344 Recent work on dementia has shown that EEG/MEG power in the delta (< 4 Hz) and theta
345 (4 – 7 Hz) frequency range is notably higher, and alpha (8 – 12 Hz) and beta markedly
346 lower, for dementia patients when compared to normal elderly subjects (Babiloniab et al.
347 2017). In particular, the dominant oscillatory frequency of the EEG spectrum for dementia
348 patients was found to be lower than for healthy controls (Peraza et al. 2018). Given that
349 dementia is believed to arise from the deterioration of synaptic connections, the synaptic
350 time scale was increased in order to model these effects. As in the schizophrenia study,
351 increasing the synaptic time scale has the effect of reducing the synaptic efficacy and
352 slowing down signal transfer. In the model, increasing the time scale decreases the
353 population synchrony and in turn the amplitude of the oscillations, for a range of spectral
354 frequencies. The increased synaptic processing time was not enough to decrease the
355 oscillatory frequency; however, this decrease may be due to an interplay between the
356 different frequency bands, which was not considered here.

357 Epilepsy is a neurological disorder characterised by seizures, periods of high amplitude and
358 highly synchronised brain oscillations. Extensive research has been carried out to design
359 treatments and preventative care for epileptic patients. However, the underlying cause of

the disorder is still unclear. Previous theoretical studies of epilepsy typically use the Jansen-Rit model (Jansen and Rit 1995), as there are parameter windows for which the model can exhibit low amplitude or high amplitude oscillations depending on the initial conditions (Wendling et al. 2001; Grimbart and Faugeras 2006; Touboul et al. 2011; Ahmadizadeh et al. 2018). However, unlike the model presented here the Jansen-Rit model cannot track neuronal synchrony. The excitatory-inhibitory two population model, given by

$$Q_{ab}g_{ab} = \kappa_{ab}f(Z_b), \quad \tau_a \frac{d}{dt}Z_a = \mathcal{F}_a(Z_a; \eta_0^a, \Lambda^a) + \sum_b \mathcal{G}(Z_a, g_{ab}; v_{\text{syn}}^{ab}), \quad (8)$$

exhibits multi-stability similar to the Jansen-Rit model. For the same parameter values, the model can exhibit fast low-amplitude oscillations (Figure 5(a)) or bursts of high-frequency activity at a slow burst rate (Figure 5(b)). Both states are stable, but perturbations can drive transitions between the states, such as a brief synaptic input to the excitatory population (Figure 5(c)). Low frequency bursts of high frequency activity (as seen in Figure 5(b)) are typical of epileptic seizures, providing further evidence that this is a suitable model for theoretical studies of epilepsy. The presence of the synchrony variable should also allow the exploration of how changes in population synchrony can lead to seizures, and help uncover protocols that would lead to seizure termination.

3 Neural mass network model

Advances in non-invasive neuroimaging methods that allow detailed characterisation of the brain's anatomy and activity, together with developments in network science, have supported a proliferation of network connectivity-based approaches, employing neural mass models as building blocks, to understand large-scale brain function. These studies are especially relevant to elucidating the emergence of *functional connectivity* (FC) networks that describe dynamic patterns of temporal coherence of activity between brain regions. Important examples include archetypal brain networks that emerge under different tasks or stimulants (Thomas Yeo et al. 2011), and so-called resting state networks (Breakspear 2017), whereby different regions of the brain's sensorimotor system oscillate slowly and synchronously in the absence of any explicit task. More generally, these FC networks are posited to support high-level brain function—the divergence between dynamic functional activity and the relatively static structural connections between populations is critical to the brain's wide functional repertoire, and may hold the key to understanding brain activity in health and disease (Park and Friston 2013; Van Den Heuvel and Pol 2010; Straaten and Stam 2013). In particular, disruptions in structural and functional brain networks are linked to a variety of psychiatric and neurological diseases such as epilepsy and schizophrenia (Braun, Muldoon, and Bassett 2015; Menon 2011).

Empirically, FC is typically derived from statistical analyses of time-series data from MEG, EEG, or functional magnetic resonance imaging (fMRI). However, while FC is widely employed in both empirical and theoretical studies, the specific link between the brain's anatomical circuitry and the varied and complex behaviour it exhibits is not fully understood (Honey, Thivierge, and Sporns 2010; Park and Friston 2013). A plethora of theoretical studies have therefore sought to elucidate SC-FC relationships, employing neural mass models, alongside anatomical connectivity networks, to simulate large-scale brain activity. These investigations have revealed, for example, strong SC-FC

402 correspondence on long time-scales, in comparison to those observed over short time-
403 scales (Honey et al. 2007, 2009; Rubinov et al. 2009) and close resemblance of structural
404 and functional networks when the neural dynamics is near a critical transition (Stam et al.
405 2016). This critical SC-FC correspondence is further highlighted in the work of Hlinka and
406 Coombes (2012), using a combination of network graph analysis and dynamical systems
407 theory to expose the role of Hopf bifurcations in the Wilson-Cowan model in organising
408 SC-FC relations; in a similar vein, multiplex clustering measures have also been exploited
409 to emphasise how SC-FC relations vary as a function of Wilson-Cowan model dynamics
410 (Crofts, Forrester, and O'Dea 2016). These ideas can be further extended to show how the
411 organisation of FC is intrinsically related to the dynamical state of the neural mass system,
412 such that FC patterns can in large parts be understood without recourse to specific
413 connectome information (Tewarie et al. 2018; Forrester et al. 2019).

414 To develop a large-scale model incorporating interconnected neural populations across the
415 whole brain, we generalise equation $Q_{ab}g_{ab} = \kappa_{ab}f(Z_b)$, $\tau_a \frac{d}{dt}Z_a = \mathcal{F}_a(Z_a; \eta_0^a, \Delta^a) +$
416 $\sum_b \mathcal{G}(Z_a, g_{ab}; v_{\text{syn}}^{ab})$, (8) to consider N connected populations of excitatory and inhibitory
417 neurons, denoted $E_1, \dots, E_N, I_1, \dots, I_N$. Therefore, for each network node m we define
418 population order parameters $Z_a \rightarrow Z_m^a$ and synaptic conductances $g_{ab} \rightarrow g_{ab}^{mn}$ for
419 $a, b \in \{E, I\}$ and $n \in \mathcal{N}(m)$, where $\mathcal{N}(m)$ denotes the set of nodes connected to node m
420 ($n = m$ represents within-node excitatory-inhibitory coupling). We note that since long-
421 range connections in the brain mainly project from excitatory pyramidal cells (Gerfen,
422 Economo, and Chandrashekhar 2018), we restrict inter-mass coupling to connections
423 between excitatory populations. Constants are denoted similarly, with
424 $(\alpha_{ab}, \kappa_{ab}, \eta_0^a, \Delta^a, v_{\text{syn}}^{ab}, \tau_a) \rightarrow (\alpha_{ab}^{mn}, \kappa_{ab}^{mn}, \eta_{0,m}^a, \Delta_m^a, v_{mn}^{ab}, \tau_m^a)$. Structural connectivity
425 between neural masses ($\kappa_{ab}^{mn}, m \neq n$) was estimated from diffusion MRI data from 10
426 subjects obtained from the Human Connectome Project (Van Essen et al. 2013). Briefly, we
427 explain how this data is post-processed to derive connectomic data, though we direct the
428 reader to Abeysuriya et al. (2018) (for related work on Wilson-Cowan neural mass
429 networks) and the references therein for a more detailed overview. 60,000 vertices on the
430 white/grey matter boundary surface for each subject (Glasser et al. 2013) were used as
431 seeds for 10,000 tractography streamlines. Streamlines were propagated through voxels
432 with up to three fibre orientations, estimated from distortion-corrected data with a
433 deconvolution model (Jbabdi et al. 2012; Sotropoulos et al. 2016), using the FSL package.
434 The number of streamlines intersecting each vertex on the boundary layer was measured
435 and normalised by the total number of valid streamlines. This resulted in a 60,000 node
436 structural matrix, which was further parcellated using the 68-node Desikan-Killiany atlas
437 (Desikan et al. 2006) (note that since each brain region is on the scale of millions of
438 neurons, they are each suitably modelled by a single neural mass). Each element of the
439 connectivity matrix κ_{ab}^{mn} ($m \neq n$) therefore reflects the proportion of white matter fibres
440 which bridge regions m and n .

441 Functional connectivity is obtained by direct simulation of this neural mass network, and
442 computing the pairwise synchronisation between time-series activity on each network
443 node, measured via the mean phase coherence (MPC; see, e.g. Mormann et al. (2000)), to
444 provide a matrix describing the strength of functional connection between each brain

445 region. Structure–function relations are assessed by computing the Jaccard similarity
446 coefficient (Jaccard 1912) of the non-diagonal entries of the binarised SC and FC matrices,
447 which provides a natural measure of matrix overlap, ranging from 0 for matrices with no
448 common links to 1 for identical matrices.

449 Results visualising both the structural and derived function networks are shown in Figure
450 6; these show how FC patterns can differ significantly from the underlying connectome
451 structure that supports neural population activity. In the following, we describe how the
452 model and approaches described above can be employed to understand the influence of
453 brain stimulation treatments on network behaviour.

454 **3.1 Transcranial magnetic stimulation**

455 Transcranial magnetic stimulation (TMS) is a non-invasive therapeutic brain stimulation
456 technique whereby strong electromagnetic fields are used to induce a transient current
457 pulse in the brain, in order to influence neural activity, particularly in superficial regions of
458 cerebral cortex. TMS has potentially wide-reaching consequences for mental health
459 conditions, having provided positive outcomes for patients with Parkinson’s disease
460 (Boggio et al. 2005; Shimamoto et al. 1999), schizophrenia (Lee et al. 2005; Lett et al. 2014)
461 and depression (Kolbinger et al. 1995; Loo and Mitchell 2005; George et al. 2000; Fox et al.
462 2012). Though its efficacy in treating these conditions, in some cases, is evident, the
463 precise neurological effects of TMS are not understood. Previous studies highlight that TMS
464 can influence neural activity within populations in a range of ways. Initial synchronous
465 depolarisation, followed by longer-lasting GABAergic inhibition (Siebner et al. 2009)
466 impacts on neuronal excitability (Lang et al. 2007) and the excitatory/inhibitory balance
467 (Iwabuchi et al. 2017), can drive neural plasticity (Fung and Robinson 2014), and alter
468 patterns of coherence between brain regions, leading to the reorganisation of functional
469 connectivity networks (Tik et al. 2017; Iwabuchi et al. 2017). Limbic structures have been
470 identified as a critical component of the pathophysiology of depression (see, e.g., Guo et al.
471 (2013), Iwabuchi et al. (2014), Mayberg (1997)), and in particular, the insula is a key part
472 of abnormalities in (Liu et al. 2010; Horn et al. 2010; Avery et al. 2014), and interactions
473 between (Mayberg 1997; Menon and Uddin 2010; Sridharan, Levitin, and Menon 2008)
474 functional networks implicated in depression. However, since TMS induces current on
475 surface regions, sub-cortical regions such as the insula must be influenced indirectly
476 (Iwabuchi et al. 2017); the mechanisms by which this occurs, and ideal stimulation
477 protocols to achieve this remain unclear. Neural mass models — and, through its account of
478 within-population synchrony, the next-generation neural mass model described herein —
479 are particularly suited to providing an understanding of how such emergent FC patterns
480 can be influenced by TMS, and interrogating the influence of TMS protocols *in silico*, to
481 inform more effective treatment.

482 TMS pulses begin with a sharp peak to induce an electric field across the cortex, causing
483 electric currents to be generated across cell membranes. This is followed by a slow
484 dissipation, resulting in a much weaker electric field in the opposite direction (Rothkegel et
485 al. 2010). Pulses may be delivered as singular bursts, or in high-frequency trains referred
486 to as repetitive TMS (rTMS). Pulses are accommodated in our neural mass network model
487 by modulating the average population drive on each node (see equation $Q_{ab}g_{ab} =$

488 $\kappa_{ab} f(Z_b), \quad \tau_a \frac{d}{dt} Z_a = \mathcal{F}_a(Z_a; \eta_0^a, \Delta^a) + \sum_b \mathcal{G}(Z_a, g_{ab}; v_{\text{syn}}^{ab}), \quad (8))$: $\eta_0^a \rightarrow \eta_{0,m}^a + H_m^a(t)$,
489 and where $a \in \{E, I\}$ and $m \in \{1, \dots, N\}$, where the function $H_m^a(t)$ is chosen to reflect the
490 particular delivery protocol. For simplicity, in the following we assume that the induced
491 drive is identical for both inhibitory and excitatory populations, with each pulse given by a
492 damped sinusoid:

493
$$H_m^a(t) = I_{\text{peak}} \sin(\omega(t - t_i)) \exp((t_i - t)/\tau) \Theta(t - t_i) \delta_{m,M}, \quad (9)$$

494 where M indicates which node (or set of nodes) is stimulated, t_i denotes pulse times, Θ the
495 Heaviside function, $I_{\text{peak}} = 100$ is the pulse amplitude (in arbitrary units), $\omega = 20\text{rad/ms}$
496 is the wave frequency and $\tau = 0.08\text{ ms}$ characterises the pulse decay time (Rusu et al.
497 2014).

498 To highlight the utility of this approach to understanding the influence of TMS on brain
499 function, we stimulated in turn each of the 14 nodes corresponding to cortical brain
500 regions, and computed the resulting FC network from simulated time-series activity on
501 each node (as described above), paying particular attention to the influence on the right
502 anterior insula. In each case, we employed an rTMS stimulation protocol at 20 Hz (George
503 et al. 1995). TMS was applied for 50 seconds; functional connectivity was computed after a
504 delay of 50 seconds post-TMS. We note that the stimulation and measurement protocol
505 adopted here was chosen for illustrative purposes rather than to mimic a TMS experiment,
506 allowing for computational efficiency and to allow for transient network activity to decay.

507 Figures Figure 7 and Figure 8 summarise our results. Figure 7 shows a representation of
508 the functional network arising from stimulation of each cortical node, interpolated onto
509 brain meshes of the right hemisphere, together with the node corresponding to the insula
510 (right hemisphere). Here, the weighted degree of each node in the FC graph was calculated
511 and normalised by highest degree. The global SC-FC similarity (measured by the Jaccard
512 similarity coefficient) is also shown. These results highlight the dramatic difference that
513 stimulating each cortical site can make to both the overall pattern of functional
514 connectivity, and the resulting influence on the insula, in particular. This is explored in
515 more detail in Figure 8, which shows the influence of each stimulated region on some
516 exemplar graph-theoretical properties, as discussed in Rubinov and Sporns (2010) and
517 Newman (2016), of the insula node (specifically, the node degree, eigencentrality and
518 clustering coefficient), together with the path-length between the stimulation site and the
519 insula. These results reemphasise the strong dependence of emergent FC on stimulation
520 site indicated in Figure 7, both in terms of global SC-FC similarity, and specific influence on
521 the insula. Moreover, the efficacy of stimulation is not strongly predicted by proximity (as
522 measured by shortest path length connecting the stimulation site, and the insula),
523 highlighting a non-trivial dependence on macroscopic brain network architecture.

524 We have shown results from a range of target regions to show the variability of simulated
525 TMS-induced FC states. However, more clinically relevant TMS protocols could be
526 implemented such as stimulation of the dorsolateral prefrontal cortex, which has
527 frequently been the subject of TMS studies related to the treatment of major depression
528 (Noda et al. 2015; Lan et al. 2016).

529

4 Neural field model

530 The structure of the neocortex is well known to have a columnar organisation (Mountcastle
531 1997), built from macrocolumns of $\sim 10^6$ neurons with similar response properties, and
532 that these tend to be vertically aligned into columnar arrangements of roughly 1 – 3 mm in
533 diameter. Intracortical connections can range over 1 – 15 cm, allowing communication
534 between distal cortical areas. Thus, it is natural to view the human cortex as a dense
535 reciprocally interconnected network of roughly 10^{10} corticocortical axonal pathways that
536 make connections within the roughly 3 mm outer layer of the cerebrum (Hagmann et al.
537 2008). Given the shallow depth of this wrinkled and folded cortical structure with a high
538 neuronal density, it is common from a modelling perspective to use a *neural field*
539 description (not to be confused with the neural mass model described earlier). This is
540 essentially a coarse-grained description of neural tissue that describes the evolution of
541 neuronal activity on a two-dimensional surface, although theoretical analyses of such
542 models are often carried out just considering one spatial dimension for simplicity. See
543 Coombes et al. (2014) for an overview. These models can incorporate large scale
544 anatomical knowledge, including the fact that most long-range synaptic interactions are
545 excitatory, with excitatory pyramidal cells sending their myelinated axons to other parts of
546 the cortex. Inhibitory interactions, on the other hand, tend to be much more short-ranged.
547 For excitatory connections it is now known that the weight of connection between two
548 areas decays exponentially with their wiring distance, with a characteristic distance of
549 ~ 11 mm (see Wang and Kennedy (2016) for a recent discussion). It is the combination of
550 *local* synaptic activity (seen in the rise and decay of post synaptic potentials with time-
551 scales from 1 – 100 ms) and *non-local* delayed interactions within the cortex (of up to 30
552 ms in humans) that is believed to be the major source of large-scale EEG and MEG signals
553 recorded at (or near) the scalp. Nunez, in particular, (Nunez 1995) has emphasised the
554 important role that delays arising from action potential propagation along corticocortical
555 fibres have in generating brain rhythms seen in the 1 – 15 Hz range. Moreover, he has
556 proposed a damped inhomogenous *brain-wave* equation describing the evolution of neural
557 activity at the tissue level that has played an important role in our understanding of waves
558 and patterns seen using EEG sensors (Nunez 1974, 1995). A recent study of the Nunez
559 model on a sphere can be found in (Visser et al. 2017), which includes an analysis of both
560 standing and rotating waves.

561 Here we describe a neural field model that generalises the basic neural mass model given
562 by $Qg = \kappa f(Z)$, (2) and $\tau \frac{d}{dt}Z = \mathcal{F}(Z; \eta_0, \Delta) +$
563 $\mathcal{G}(Z, g; v_{\text{syn}})$, (4) to include both the spatial extent of anatomical
564 interactions and the axonal delays that arise. Symbolically we write this in the form $Qg =$
565 $\psi, \psi = w \otimes f(Z)$, where Q and Z are given as before, though here $(g, Z) = (g(\mathbf{r}, t), Z(\mathbf{r}, t))$,
566 where \mathbf{r} indicates a position within the cortical surface (and for simplicity this is treated as
567 a sheet with no depth). The symbol \otimes is used to describe spatial interaction within the
568 neural field model, whilst w represents structural connectivity. For example, for an
569 idealised one-dimensional setting with $\mathbf{r} = x \in \mathbb{R}$ then we might consider

570
$$[w \otimes f(Z)](x, t) = \int_{\mathbb{R}} dy w(|x - y|)f \circ Z(y, t - |x - y|/v). \quad (10)$$

571 Here the anatomical connectivity is described by the distance dependent function w , and
 572 axonal transmission delays are prescribed solely in terms of this distance and a uniform
 573 axonal speed v . If the former has the normalised exponential dependence, $w(x) =$
 574 $\exp(-|x|/\sigma)/(2\sigma)$ then there is an equivalent partial differential equation (Jirsa and Haken
 575 1997)

$$576 \quad \left[\left(\frac{1}{\sigma} + \frac{1}{v} \frac{\partial}{\partial t} \right)^2 - \frac{\partial^2}{\partial x^2} \right] \psi = \frac{1}{\sigma} \left(\frac{1}{\sigma} + \frac{1}{v} \frac{\partial}{\partial t} \right) f \circ Z. \quad (11)$$

576 $1\sigma+1v\partial\partial t2-\partial2\partial x2\psi=1\sigma1\sigma+1v\partial\partial tf\circ Z.$ (11) and the original brain
 648 wave equation of Nunez (1974) is that here f is given by $f(Z) = \frac{1}{\pi\tau} \operatorname{Re} \left(\frac{1-Z^*}{1+Z^*} \right)$

649
 650 (1). The Nunez model of EEG respects the physiology and anatomy
 651 described above and has been particularly successful for describing standing EEG waves
 652 that arise by interference in a system with periodic boundary conditions. In a planar
 653 system with a rotationally symmetric anatomical connectivity described by $w(r) =$
 654 $\exp(-r/\sigma)/(2\pi\sigma^2)$ the corresponding brain wave equation is

$$655 \quad \left[\left(\frac{1}{\sigma} + \frac{1}{v} \frac{\partial}{\partial t} \right)^2 - \frac{3}{2} \nabla^2 \right] \psi = \frac{1}{\sigma^2} f \circ Z. \quad (12)$$

656 Unlike $\left[\left(\frac{1}{\sigma} + \frac{1}{v} \frac{\partial}{\partial t} \right)^2 - \frac{\partial^2}{\partial x^2} \right] \psi = \frac{1}{\sigma} \left(\frac{1}{\sigma} + \frac{1}{v} \frac{\partial}{\partial t} \right) f \circ Z.$ (11), the wave
 657 equation given by $\left[\left(\frac{1}{\sigma} + \frac{1}{v} \frac{\partial}{\partial t} \right)^2 - \frac{3}{2} \nabla^2 \right] \psi = \frac{1}{\sigma^2} f \circ Z.$ (12) is only
 658 strictly valid for describing *long-wavelength* solutions. In general, we can avoid the
 659 assumptions that go into using brain wave equations by working directly with the integral
 660 form of ψ . This can be posed on a realistic cortical surface Ω and written as

$$661 \quad \psi(\mathbf{r}, t) = \int_{\Omega} d\mathbf{r}' W(\mathbf{r}, \mathbf{r}') f \circ Z(\mathbf{r}', t - \tau(\mathbf{r}, \mathbf{r}')), \quad (13)$$

662 where the kernels W and τ allow for more general structural and delayed interactions.

663 In the above discussion we have only considered long range interactions that are
 664 excitatory. However, in real cortical tissue metabolic processes would act to limit sustained
 665 high firing rates. A simple model of such so-called *spike frequency adaptation* can be
 666 developed by replacing the mean drive η_0 by $\eta_0 - \delta a$, for some positive strength of
 667 feedback $\delta > 0$ coupled to an adaptation field a . This in turn is driven by the firing rate of
 668 the tissue:

$$669 \quad \tau_A \frac{\partial a}{\partial t} = f \circ Z - a. \quad (14)$$

670 This form of feedback can also be interpreted as a form of localised synaptic inhibitory
 671 feedback. In terms of its effect on a travelling wave the main action of this feedback would
 672 be to turn an otherwise travelling front into a travelling pulse of neural activity. A recent
 777 $\otimes f Z x, t = R d y w x - y f \circ Z y, t - x - y / v.$ (10) in the absence of axonal delays and
 778 adaptation has been given in Byrne, Avitabile and Coombes (2019). In this paper it was
 779 shown that the model supports a Turing instability (of a homogeneous steady state), that
 780 can lead to the formation of travelling waves, with properties not seen in standard neural

781 field models. The main one being the dynamic evolution of population synchrony within
782 travelling fronts and pulses, as typically seen in networks of spiking neurons. We now turn
783 to the use of the above models, with axonal delays and adaptation, in interpreting and
784 understanding the dynamics of cortical waves as observed in neuroimaging studies.
785 However, it is well to note that other reductions of spiking (linear IF) networks to neural
786 field models are also possible, typically assuming a 'balance' of excitation and inhibition,
787 that can also give a better account of network dynamics than phenomenological neural
788 field models, and see e.g. Rosenbaum and Doiron (2014), Pyle and Rosenbaum (2017).

789 4.1 Cortical wave simulations

790 Travelling waves at the scale of the whole brain have been studied ever since the advent of
791 EEG, with more recent studies progressing with the use of electrocorticography (ECoG), in
792 which arrays of electrodes are placed directly on the cortical surface. Both EEG and ECoG
793 indicate that wave speeds are typically in the 1 – 10 m/s range (consistent with the axonal
794 conduction speeds of myelinated cortical white matter fibres). The development of multi-
795 electrode array and voltage-sensitive dye imaging techniques has brought us even more
796 information about their spatio-temporal properties and shown that they are present during
797 almost every type of cortical processing (Wu, Huang, and Zhang 2008). Waves can occur
798 during both awake and sleep states and can range over both small and large cortical spatial
799 scales. Moreover, they can also occur during pathological states, such as seizures and
800 spreading depression. For a recent discussion of the mechanisms underlying cortical wave
801 propagation, as well as their role in computation, see Muller et al. (2018).

802 The treatment of macroscopic cortical waves is best studied from a theoretical perspective
803 with a wave equation describing the evolution of neural activity at the tissue level. The next
804 $1\sigma + 1\nu \partial \partial t^2 - \partial^2 \partial x^2 \psi = 1\sigma 1\sigma + 1\nu \partial \partial t f \circ Z.$ (11) and

1000 $1\sigma + 1\nu \partial \partial t^2 - 32\nabla^2 \psi = 1\sigma 2f \circ Z.$ (12) are ideal candidates. Here we
1001 $\tau A \partial a \partial t = f \circ Z - a.$ (14), with a focus on the speed and shape

1176 $1\sigma + 1\nu \partial \partial t^2 - \partial^2 \partial x^2 \psi = 1\sigma 1\sigma + 1\nu \partial \partial t f \circ Z.$ (11) to study a travelling
1177 wave of activity. Figure 9 shows that the pulse speed increases linearly with axonal speed ν
1178 for very small ν , and then saturates to a constant value relatively quickly. The shape of the
1179 wave is a localised pulse in the conductance variable g , with interesting substructures in
1180 the order parameter $Z = Re^{i\Psi}$ within a pulse. The two insets show the variation of R (the
1181 degree of synchrony) and Ψ (its phase) across the wave pulse.

1250 $1\sigma + 1\nu \partial \partial t^2 - 32\nabla^2 \psi = 1\sigma 2f \circ Z.$ (12), and in this case expect to see
1251 the radially symmetric counterpart of a travelling pulse in the form of a spreading circular
1252 ring, reminiscent of an ictal wavefront (Schevon et al. 2012), as shown in Figure 10. This is
1253 initiated by a localised and transient external input. The internal dynamics for Z within a
1254 radial cross section through the ring of activity shown is reminiscent of that seen in a one-
1255 dimensional travelling pulse.

1281 In many neuroimaging studies of brain waves, authors have reported interesting phase
1282 relationships across cortical domains. For example, Alexander et al. (2016) have observed
1283 travelling phase waves at the level of the whole head using MEG (during an observer-
1284 triggered apparent motion task), and Denker et al. (2018) have used multi-electrode arrays

1285 to quantify planar, synchronised, random, circular, and radial phase patterns in monkey
1286 primary motor cortex. The establishment of phase relationships necessarily requires local
1287 oscillations. These can be achieved within the modelling framework presented here in one
1288 of two natural ways. The first exploits the fact that in known parameter regimes the point
1289 neural mass model can oscillate, either via a Hopf bifurcation or through an isola of limit-
1290 cycles (Coombes and Byrne 2019). The second utilises the fact that even for standard
1291 neural field models with axonal delays that a mixture of short-range inhibition and long-
1292 range excitation can lead to a *dynamic Turing instability* underlying the formation of
1293 periodic travelling waves (Coombes et al. 2007). These generate a phase-relationship
1294 between oscillations at different points in the cortical tissue. This second mechanism
1295 requires the coupling of brain wave equations, one for each type of synaptic conductance
1296 mediating the interaction between excitatory and inhibitory populations (using the
1401 $Q_{ab}g_{ab} = \kappa a b f Z_b$, $\tau_{add} t Z_a = F_a Z_a; \eta_0 a, \Delta a + b G Z_a, g_{ab}; v_{syn} ab$, (8), though for
1402 brevity we shall not pursue this further here.

1403 5 Discussion

1404 In the last 50 years there has been an active take-up of modelling approaches in the
1405 neurosciences, with many of these inspired by the research activity of Jack Cowan. The next
1406 generation neural activity models and their application presented here are a case in point
1407 and can trace their scientific roots back to the Wilson–Cowan model. In the spirit of the
1408 original Wilson–Cowan model we have reviewed a recent neural mass model for describing
1409 the population activity of mesoscopic collections of neurons, and its extension to
1410 macroscopic large-scale networks, both discrete and continuum. The local model is ideally
1411 suited to studying phenomenon such as event related synchrony/de-synchrony, the
1412 discrete network can naturally address the link between structural and functional
1413 connectivity, and the continuum model is suited to understanding the properties of cortical
1414 wave propagation. In contrast to the Wilson–Cowan model, the one considered here can be
1415 derived from an underlying microscopic description of a spiking cell. Admittedly, this is for
1416 a specific choice of idealised quadratic integrate-and-fire model, for which the
1417 mathematical Ott–Antonsen reduction holds. However, as a common choice for a model of a
1418 cortical cell (given its ability to fire at low rate) this is a fortuitous circumstance. Although
1419 the search for other mean-field models linked to different choices of single neuron model is
1420 of deep mathematical interest, there is clearly a lot of mileage yet to be had in the study and
1421 application of the next generation models presented here. It is well to mention a few of
1422 these possibilities below.

1423 The first application considered in this paper was to post-movement beta rebound and
1424 movement related beta decrease. For simplicity we assumed that these were both
1425 mediated by the same type of synaptic receptor. However, Hall et al. (2011) suggest that
1426 movement related beta decrease is a GABA-A mediated process, whilst post-movement
1427 beta rebound appears to be generated by a non-GABA-A receptor mediated process. A
1428 further model that distinguishes between receptors, may offer important insights into
1429 motor processes, and can be readily accommodated within the framework that we have
1430 presented here. In the simple two node hemisphere model, the magnitude and length of

1431 beta rebound was heavily dependent on the oscillatory phase at which the motor command
1432 was applied. This trial-by-trial variability is also true of MEG recording of beta-rebound.
1433 Current analysis techniques often remove phase information from recorded MEG activity.
1434 However, it is possible to extract this information and test if there is a correlation between
1435 the phase of the beta oscillations and the magnitude/length of beta rebound, on a trial-by-
1436 trial basis. The phase coherence between the right and left hemispheres would also be an
1437 interesting measure to test for correlations. Furthermore, for the beta rebound study we
1438 have focused on simple networks built from one or a few nodes, and another intriguing
1439 study would be to explore the spread of beta rebound processes across the cortex, using
1440 the neural field formulation.

1441 The second application focused on the use of a neural mass network model (incorporating
1442 human connectome data) to relate structural and functional connectivity, and the
1443 subsequent use of the same network framework to understand the influence of
1444 transcranial magnetic stimulation on brain dynamics. This modelling approach would also
1445 seem relevant to developing an understanding of treatments for Parkinson's disease. This
1446 is a neurodegenerative disorder characterised by excessive synchronisation in the basal
1447 ganglia. Deep brain stimulation, the most common surgical intervention for treating
1448 Parkinson's disease, acts to disrupt the high levels of synchrony in the basal ganglia by
1449 administering brief pulses of electrical current through the implanted electrodes. This has
1450 proven exceptionally powerful in treating the symptoms of Parkinson's disease, yet its
1451 success remains poorly understood (Schulz, Hausmann, and Hardy 2016). Understanding
1452 how electrical pulses can disrupt population synchrony and maintain the basal ganglia in
1453 an asynchronous state could prove essential for fine tuning deep brain stimulation
1454 protocols and providing more effective treatments to Parkinson's patients. Given the ability
1455 of the model to track within-population synchrony in a tractable way, it is an ideal
1456 candidate for a theoretical study of deep brain stimulation. Similarly, there is much further
1457 work to be done on using the network model to gain further insight into the effectiveness
1458 of transcranial magnetic stimulation protocols in influencing neural states, especially as
1459 regards transient neurodisruption (Siebner et al. 2009) and state-dependent effects
1460 (Pasley, Allen, and Freeman 2009). Moreover, in this regard it is especially important to
1461 consider the development of a sub-cortical model of the thalamus, and the inclusion of
1462 thalamocortical connectivity. From a modelling perspective this would require a
1463 description of some of the important nonlinear ionic currents known to shape the firing
1464 pattern of thalamocortical relay cells and reticular cells (Destexhe and Sejnowski 2001). A
1465 neural mass that incorporates one such important current, the slow T-type Calcium
1466 current, has previously been developed by Coombes (2003), and next steps could involve a
1467 hybrid network that couples this with the next generation model presented here.

1468 The third and final application considered was to whole brain dynamics, and specifically to
1469 cortical waves using a generalisation of the brain-wave equation. The study of waves, their
1470 initiation, and their interactions is especially pertinent to the study of epileptic brain
1471 seizures. However, it is known that gap junctions are especially important in this instance
1472 (Martinet et al. 2017), and an important extension of the work presented here is their
1473 inclusion in the modelling framework. Laing (2015) has already made major inroads on
1474 this challenge, and it would be extremely interesting to pursue the translation of this

1475 theoretical work to understand how gap junctions may contribute to the generation of
1476 spatio-temporal neural rhythms, both functional (Hormuzdi et al. 2004; Bennet and Zukin
1477 2004) and pathological (Velazquez and Carlen 2000; Dudek 2002).

1478 Finally, it is well to mention that the work presented here has ignored any form of plasticity
1479 (Zucker and Regehr 2002), and this almost certainly has an impact on general aspects of
1480 brain dynamics such as synchronisation and travelling waves (Lubenov and Siapas 2008),
1481 and more specifically on the extensions mentioned above that concern the brain response
1482 to transcranial magnetic stimulation and the network dynamics that arise in epilepsy.
1483 Given that the next generation model presented here incorporates a conductance-based
1484 model of the synapse (with reversal potential and bi-exponential temporal response) this
1485 can be modulated in a meaningful way to describe various forms of plasticity. As well as
1486 incorporating long-term plasticity, say following the route by Robinson for Wilson-Cowan
1487 models (Robinson 2011) (and already realised for its importance in transcranial magnetic
1488 stimulation (Fung and Robinson 2014)), it is also possible to augment the model to treat
1489 homeostatic plasticity as advocated by Vogels et al. (2011) and Hellyer et al. (2016), and
1490 already implemented in Abeysuriya et al. (2018) for Wilson-Cowan models. Short-term
1491 plasticity has previously been incorporated into neural field models by several authors,
1492 mainly through a simple facilitation/depression description as in Kilpatrick and Bressloff
1493 (2010), Mi, Lin and Wu (2016) and Kilpatrick (2018), and can also be naturally included in
1494 future studies.

1495 Acknowledgements

1496 Áine Byrne was funded by the Swartz Foundation on a postdoctoral fellowship. Michael
1497 Forrester would like to acknowledge the Beacon in Precision Imaging at the University of
1498 Nottingham for financial support during the completion of this work.

1499 References

- 1500 Abeysuriya, Romesh G, Jonathan Hadida, Stamatis N Sotiropoulos, Saad Jbabdi, Robert
1501 Becker, Benjamin AE Hunt, Matthew J Brookes, and Mark W Woolrich. 2018. "A Biophysical
1502 Model of Dynamic Balancing of Excitation and Inhibition in Fast Oscillatory Large-Scale
1503 Networks." *PLoS Computational Biology* 14 (2). Public Library of Science: e1006007.
- 1504 Ahmadizadeh, Saeed, Philippa J. Karoly, Dragan Nešić, David B. Grayden, Mark J. Cook,
1505 Daniel Soudry, and Dean R. Freestone. 2018. "Bifurcation analysis of two coupled Jansen-
1506 Rit neural mass models." Edited by Gennady Cymbalyuk. *PLOS ONE* 13 (3). Public Library of
1507 Science: e0192842. <https://doi.org/10.1371/journal.pone.0192842>.
- 1508 Alexander, Andrey R. AND Jurica, David M. AND Nikolaev. 2016. "Global Neuromagnetic
1509 Cortical Fields Have Non-Zero Velocity." *PLOS ONE* 11 (3). Public Library of Science: 1–29.
1510 <https://doi.org/10.1371/journal.pone.0148413>.
- 1511 Anderson, J A, and E Rosenfeld. 1998. "Talking Nets: An Oral History of Neural Networks."
1512 In, edited by J A Anderson and E Rosenfeld. Cambridge, Massachusetts: MIT Press.

- 1513 Avery, Jason A, Wayne C Drevets, Scott E Moseman, Jerzy Bodurka, Joel C Barcalow, and W
1514 Kyle Simmons. 2014. "Major Depressive Disorder Is Associated with Abnormal
1515 Interoceptive Activity and Functional Connectivity in the Insula." *Biological Psychiatry* 76.
1516 Elsevier: 258–66.
- 1517 Babiloniab, C, C Del Percioc, R Lizio, G Noce, S Cordone, S Lopez, A Soricelli, et al. 2017.
1518 "Abnormalities of cortical neural synchronization mechanisms in patients with dementia
1519 due to Alzheimer's and Lewy body diseases: an EEG study." *Neurobiology of Aging* 55.
1520 Elsevier: 143–58.
1521 <https://www.sciencedirect.com/science/article/pii/S0197458017301136?via%20Dihub>
1522 .
- 1523 Bennet, M V L, and R S Zukin. 2004. "Electrical Coupling and Neuronal Synchronization in
1524 the Mammalian Brain." *Neuron* 41: 495–511.
- 1525 Beurle, R L. 1956. "Properties of a Mass of Cells Capable of Regenerating Pulses."
1526 *Philosophical Transactions of the Royal Society London B* 240: 55–94.
- 1527 Boggio, Paulo S, Felipe Fregni, Felix Bermpohl, Carlos G Mansur, Moacyr Rosa, Demetrio O
1528 Rumi, Egberto R Barbosa, et al. 2005. "Effect of Repetitive TMS and Fluoxetine on Cognitive
1529 Function in Patients with Parkinson's Disease and Concurrent Depression." *Movement
1530 Disorders: Official Journal of the Movement Disorder Society* 20. Wiley Online Library: 1178–
1531 84.
- 1532 Braun, Urs, Sarah F Muldoon, and Danielle S Bassett. 2015. "On Human Brain Networks in
1533 Health and Disease." *eLS*. John Wiley & Sons, 1–9.
- 1534 Breakspear, M. 2017. "Dynamic Models of Large-Scale Brain Activity." *Nature Neuroscience*
1535 20: 340–52.
- 1536 Breakspear, Michael, Stewart Heitmann, and Andreas Daffertshofer. 2010. "Generative
1537 Models of Cortical Oscillations: Neurobiological Implications of the Kuramoto Model."
1538 *Frontiers in Human Neuroscience* 4: 190.
- 1539 Bressloff, P C, J D Cowan, M Golubitsky, P J Thomas, and M C Wiener. 2001. "Geometric
1540 visual hallucinations, Euclidean symmetry and the functional architecture of striate cortex."
1541 *Philosophical Transactions of the Royal Society of London. Series B, Biological Sciences* 356:
1542 299–330.
- 1543 Buzsáki, G. 2011. *Rhythms of the Brain*. Oxford University Press.
- 1544 Byrne, Á, D Avitabile, and S Coombes. 2019. "A Next Generation Neural Field Model: The
1545 Evolution of Synchrony Within Patterns and Waves." *Physical Review E* 99: 012313.
- 1546 Byrne, Á, M J Brookes, and S Coombes. 2017. "A Mean Field Model for Movement Induced
1547 Changes in the Beta Rhythm." *Journal of Computational Neuroscience* 43: 143–58.
- 1548 Byrne, Á, S Coombes, and P F Liddle. 2019. "Handbook of Multi-Scale Models of Brain
1549 Disorders." In, edited by V Cutsuridis. Springer.

- 1550 Coombes, S. 2003. "Dynamics of Synaptically Coupled Integrate-and-Fire-or-Burst
1551 Neurons." *Physical Review E* 67: 041910.
- 1552 Coombes, S, and A Byrne. 2019. "Lecture Notes Nonlinear Dynamics in Computational
1553 Neuroscience: from Physics and Biology to ICT." In, edited by A Torcini and F Corinto, 1–16.
1554 PoliTO. Springer.
- 1555 Coombes, S, Y-M Lai, M Sayli, and R Thul. 2018. "Networks of Piecewise Linear Neural Mass
1556 Models." *European Journal of Applied Mathematics* 29: 869–90.
- 1557 Coombes, Stephen, P. (Peter) Beim Graben, Roland Potthast, and James Wright. 2014.
1558 *Neural fields : Theory and Applications*. Springer.
- 1559 Coombes, S, N A Venkov, L Shiau, I Bojak, D T J Liley, and C R Laing. 2007. "Modeling
1560 Electrocortical Activity Through Improved Local Approximations of Integral Neural Field
1561 Equations." *Physical Review E* 76: 051901–8.
- 1562 Cowan, J D, and G B Ermentrout. 1978. "Mathematics in Biology." In, edited by S Levin.
1563 Washington DC: Mathematical Association of America.
- 1564 Crofts, Jonathan J, Michael Forrester, and Reuben D O'Dea. 2016. "Structure-Function
1565 Clustering in Multiplex Brain Networks." *EPL (Europhysics Letters)* 116 (1). IOP Publishing:
1566 18003.
- 1567 Denker, M, L Zehl, B E Kilavik, M Diesmann, T Brochier, A Riehle, and S Grün. 2018. "LFP
1568 Beta Amplitude Is Linked to Mesoscopic Spatio-Temporal Phase Patterns." *Scientific
1569 Reports* 8 (1): 5200. <https://doi.org/10.1038/s41598-018-22990-7>.
- 1570 Desikan, Rahul S, Florent Ségonne, Bruce Fischl, Brian T Quinn, Bradford C Dickerson,
1571 Deborah Blacker, Randy L Buckner, et al. 2006. "An Automated Labeling System for
1572 Subdividing the Human Cerebral Cortex on MRI Scans into Gyral Based Regions of Interest."
1573 *NeuroImage* 31. Elsevier: 968–80.
- 1574 Destexhe, A, and T Sejnowski. 2001. *Thalamocortical Assemblies: How Ion Channels, Single
1575 Neurons and large-Scale Networks Organize Sleep Oscillations*. Monographs of the
1576 Physiological Society. Oxford University Press.
- 1577 Destexhe, A, and T J Sejnowski. 2009. "The Wilson–Cowan Model, 36 Years Later."
1578 *Biological Cybernetics* 101: 1–2.
- 1579 Dudek, F E. 2002. "Gap Junctions and Fast Oscillations: A Role in Seizures and
1580 Epileptogenesis?" *Epilepsy Currents* 2: 133–36.
- 1581 Erlhagen, W, and G Schoner. 2002. "Dynamic Field Theory of Movement Preparation."
1582 *Psychological Reviews* 109: 545–72.
- 1583 Ermentrout, B, and J D Cowan. 1979. "Temporal Oscillations in Neuronal Nets." *Journal of
1584 Mathematical Biology* 7: 265–80.

- 1585 Ermentrout, G B, and J D Cowan. 1979a. "A mathematical theory of visual hallucination
1586 patterns." *Biological Cybernetics* 34: 137–50.
- 1587 Ermentrout, G B, and J D Cowan. 1980. "Large Scale Spatially Organized Activity in Neural
1588 Nets." *SIAM Journal on Applied Mathematics* 38 (1).
- 1589 Feingold, J, D J Gibson, B De Pasquale, and A M Graybiel. 2015. "Bursts of Beta Oscillation
1590 Differentiate Postperformance Activity in the Striatum and Motor Cortex of Monkeys
1591 Performing Movement Tasks." *Proceedings of the National Academy of Sciences* 112: 13687–
1592 92.
- 1593 Forrester, Michael, Stephen Coombes, Jonathan J. Crofts, Stamatios N. Sotiropoulos, and
1594 Reuben D. O'Dea. 2019. "The role of node dynamics in shaping emergent functional
1595 connectivity patterns in the brain." *arXiv E-Prints*, June, arXiv:1906.11573.
- 1596 Fox, Michael D, Randy L Buckner, Matthew P White, Michael D Greicius, and Alvaro Pascual-
1597 Leone. 2012. "Efficacy of Transcranial Magnetic Stimulation Targets for Depression Is
1598 Related to Intrinsic Functional Connectivity with the Subgenual Cingulate." *Biological
1599 Psychiatry* 72. Elsevier: 595–603.
- 1600 Fries, P. 2005. "A Mechanism for Cognitive Dynamics: Neuronal Communication Through
1601 Neuronal Coherence." *Trends in Cognitive Sciences* 9: 474–80.
- 1602 Fung, PK, and PA Robinson. 2014. "Neural Field Theory of Synaptic Metaplasticity with
1603 Applications to Theta Burst Stimulation." *Journal of Theoretical Biology* 340. Elsevier: 164–
1604 76.
- 1605 George, Mark S, Ziad Nahas, Monica Molloy, Andrew M Speer, Nicholas C Oliver, Xing-Bao
1606 Li, George W Arana, S Craig Risch, and James C Ballenger. 2000. "A Controlled Trial of Daily
1607 Left Prefrontal Cortex TMS for Treating Depression." *Biological Psychiatry* 48. Elsevier:
1608 962–70.
- 1609 George, Mark S, Eric M Wassermann, Wendol A Williams, Ann Callahan, Terence A Ketter,
1610 Peter Basser, Mark Hallett, and Robert M Post. 1995. "Daily Repetitive Transcranial
1611 Magnetic Stimulation (rTMS) Improves Mood in Depression." *Neuroreport: An International
1612 Journal for the Rapid Communication of Research in Neuroscience* 2. Lippincott Williams &
1613 Wilkins: 1853–6.
- 1614 Gerfen, Charles R, Michael N Economo, and Jayaram Chandrashekhar. 2018. "Long Distance
1615 Projections of Cortical Pyramidal Neurons." *Journal of Neuroscience Research* 96. Wiley
1616 Online Library: 1467–75.
- 1617 Glasser, Matthew F, Stamatios N Sotiropoulos, J Anthony Wilson, Timothy S Coalson, Bruce
1618 Fischl, Jesper L Andersson, Junqian Xu, et al. 2013. "The Minimal Preprocessing Pipelines
1619 for the Human Connectome Project." *NeuroImage* 80. Elsevier: 105–24.
- 1620 Grimbert, François, and Olivier Faugeras. 2006. "Bifurcation Analysis of Jansen's Neural
1621 Mass Model." *Neural Computation* 18 (12). MIT Press 238 Main St., Suite 500, Cambridge,

- 1622 MA 02142-1046 USA journals-info@mit.edu: 3052-68.
1623 <https://doi.org/10.1162/neco.2006.18.12.3052>.
- 1624 Guo, Shuixia, Yun Yu, Jie Zhang, and Jianfeng Feng. 2013. "A Reversal Coarse-Grained
1625 Analysis with Application to an Altered Functional Circuit in Depression." *Brain and*
1626 *Behavior* 3. Wiley Online Library: 637-48.
- 1627 Hagmann, P, L Cammoun, X Gigandet, R Meuli, C J Honey, and V J Weeden. 2008. "Mapping
1628 the Structural Core of Human Cerebral Cortex." *PLoS Biology* 6: e159.
- 1629 Hall, S D, I M Stanford, N Yamawaki, C J McAllister, K C Rönnqvist, G L Woodhall, and P L
1630 Furlong. 2011. "The Role of GABAergic Modulation in Motor Function Related Neuronal
1631 Network Activity." *NeuroImage* 56: 1506-10.
1632 <https://doi.org/https://doi.org/10.1016/j.neuroimage.2011.02.025>.
- 1633 Hellyer, P J, B Jachs, C Clopath, and R Leech. 2016. "Local Inhibitory Plasticity Tunes
1634 Macroscopic Brain Dynamics and Allows the Emergence of Functional Brain Networks."
1635 *NeuroImage* 124: 85-95.
- 1636 Hlinka, Jaroslav, and Stephen Coombes. 2012. "Using Computational Models to Relate
1637 Structural and Functional Brain Connectivity." *European Journal of Neuroscience* 36 (2).
1638 Wiley Online Library: 2137-45.
- 1639 Honey, Christopher J, Rolf Kötter, Michael Breakspear, and Olaf Sporns. 2007. "Network
1640 Structure of Cerebral Cortex Shapes Functional Connectivity on Multiple Time Scales."
1641 *Proceedings of the National Academy of Sciences* 104 (24). National Acad Sciences: 10240-5.
- 1642 Honey, Christopher J, Jean-Philippe Thivierge, and Olaf Sporns. 2010. "Can Structure
1643 Predict Function in the Human Brain?" *NeuroImage* 52 (3). Elsevier: 766-76.
- 1644 Honey, CJ, O Sporns, Leila Cammoun, Xavier Gigandet, Jean-Philippe Thiran, Reto Meuli, and
1645 Patric Hagmann. 2009. "Predicting Human Resting-State Functional Connectivity from
1646 Structural Connectivity." *Proceedings of the National Academy of Sciences* 106 (6). National
1647 Acad Sciences: 2035-40.
- 1648 Hormuzdi, S G, M A Filippov, G Mitropoulou, H Monyer, and R Bruzzone. 2004. "Electrical
1649 Synapses: A Dynamic Signaling System That Shapes the Activity of Neuronal Networks."
1650 *Biochimica et Biophysica Acta* 1662: 113-37.
- 1651 Horn, Dorothea I, Chunshui Yu, Johann Steiner, Julia Buchmann, Joern Kaufmann,
1652 Annemarie Osoba, Ulf Eckert, et al. 2010. "Glutamatergic and Resting-State Functional
1653 Connectivity Correlates of Severity in Major Depression—the Role of Pregenual Anterior
1654 Cingulate Cortex and Anterior Insula." *Frontiers in Systems Neuroscience* 4. Frontiers: 33.
- 1655 Iwabuchi, Sarina J, Daihui Peng, Yiru Fang, Kaida Jiang, Elizabeth B Liddle, Peter F Liddle,
1656 and Lena Palaniyappan. 2014. "Alterations in Effective Connectivity Anchored on the Insula
1657 in Major Depressive Disorder." *European Neuropsychopharmacology* 24. Elsevier: 1784-92.

- 1658 Iwabuchi, Sarina J, Felix Raschke, Dorothee P Auer, Peter F Liddle, Sudheer T Lankappa, and
1659 Lena Palaniyappan. 2017. "Targeted Transcranial Theta-Burst Stimulation Alters Fronto-
1660 Insular Network and Prefrontal GABA." *NeuroImage* 146. Elsevier: 395–403.
- 1661 Jaccard, Paul. 1912. "The Distribution of the Flora in the Alpine Zone. 1." *New Phytologist*
1662 11. Wiley Online Library: 37–50.
- 1663 Jansen, Ben H., and Vincent G. Rit. 1995. "Electroencephalogram and visual evoked
1664 potential generation in a mathematical model of coupled cortical columns." *Biological
1665 Cybernetics* 73. Springer-Verlag: 357–66. <https://doi.org/10.1007/BF00199471>.
- 1666 Jansen, B H, and V G Rit. 1995. "Electroencephalogram and Visual Evoked Potential
1667 Generation in a Mathematical Model of Coupled Cortical Columns." *Biological Cybernetics*
1668 73: 357–66.
- 1669 Jbabdi, Saad, Stamatis N Sotiroopoulos, Alexander M Savio, Manuel Graña, and Timothy EJ
1670 Behrens. 2012. "Model-Based Analysis of Multishell Diffusion MR Data for Tractography:
1671 How to Get over Fitting Problems." *Magnetic Resonance in Medicine* 68. Wiley Online
1672 Library: 1846–55.
- 1673 Jirsa, V K, and H Haken. 1997. "A Derivation of a Macroscopic Field Theory of the Brain
1674 from the Quasi-Microscopic Neural Dynamics." *Physica D* 99: 503–26.
- 1675 Kilpatrick, Z P. 2018. "Synaptic Mechanisms of Interference in Working Memory." *Scientific
1676 Reports* 8: 7879.
- 1677 Kilpatrick, Z P, and P C Bressloff. 2010. "Effects of Synaptic Depression and Adaptation on
1678 Spatiotemporal Dynamics of an Excitatory Neuronal Network." *Physica D* 239: 547–60.
- 1679 Kolbinger, Hans Martin, Gereon Höflich, Andreas Hufnagel, Hans-Jürgen Müller, and
1680 Siegfried Kasper. 1995. "Transcranial Magnetic Stimulation (TMS) in the Treatment of
1681 Major Depression — a Pilot Study." *Human Psychopharmacology: Clinical and Experimental*
1682 10. Wiley Online Library: 305–10.
- 1683 Laing, C R. 2015. "Exact Neural Fields Incorporating Gap Junctions." *SIAM Journal on Applied
1684 Dynamical Systems* 14: 1899–1929.
- 1685 Lan, M J, B T Chhetry, C Liston, J J Mann, and M Dubin. 2016. "Transcranial Magnetic
1686 Stimulation of Left Dorsolateral Prefrontal Cortex Induces Brain Morphological Changes in
1687 Regions Associated with a Treatment Resistant Major Depressive Episode: An Exploratory
1688 Analysis." *Brain Stimulation* 9: 577–83.
- 1689 Lang, Nicolas, Hartwig R Siebner, Zoltan Chadaide, Klara Boros, Michael A Nitsche, John C
1690 Rothwell, Walter Paulus, and Andrea Antal. 2007. "Bidirectional modulation of primary
1691 visual cortex excitability: a combined tDCS and rTMS study." *Investigative Ophthalmology &
1692 Visual Science* 48. The Association for Research in Vision; Ophthalmology: 5782–7.
- 1693 Lea-Carnall, C A, M A Montemurro, N J Trujillo-Barreto, L M Parkes, and W El-Deredy. 2016.
1694 "Cortical Resonance Frequencies Emerge from Network Size and Connectivity." *PLoS*

- 1695 *Computational Biology* 12. Public Library of Science: 1–19.
1696 <https://doi.org/10.1371/journal.pcbi.1004740>.
- 1697 Lee, Seung-Hwan, Won Kim, Young-Cho Chung, Kyung-Hee Jung, Won-Myong Bahk, Tae-
1698 Yun Jun, Kwang-Soo Kim, Mark S George, and Jeong-Ho Chae. 2005. “A double blind study
1699 showing that two weeks of daily repetitive TMS over the left or right temporoparietal
1700 cortex reduces symptoms in patients with schizophrenia who are having treatment-
1701 refractory auditory hallucinations.” *Neuroscience Letters* 376. Elsevier: 177–81.
- 1702 Lett, Tristram A, Aristotle N Voineskos, James L Kennedy, Brian Levine, and Zafiris J
1703 Daskalakis. 2014. “Treating Working Memory Deficits in Schizophrenia: A Review of the
1704 Neurobiology.” *Biological Psychiatry* 75. Elsevier: 361–70.
- 1705 Liley, D T J, P J Cadusch, and M P Dafilis. 2002. “A Spatially Continuous Mean Field Theory of
1706 Electrocortical Activity.” *Network* 13: 67–113.
- 1707 Liu, Zhifen, Cheng Xu, Yong Xu, Yanfang Wang, Bing Zhao, Yating Lv, Xiaohua Cao, Kerang
1708 Zhang, and Chongxi Du. 2010. “Decreased Regional Homogeneity in Insula and Cerebellum:
1709 A Resting-State fMRI Study in Patients with Major Depression and Subjects at High Risk for
1710 Major Depression.” *Psychiatry Research: Neuroimaging* 182. Elsevier: 211–15.
- 1711 Loo, Colleen K, and Philip B Mitchell. 2005. “A review of the efficacy of transcranial
1712 magnetic stimulation (TMS) treatment for depression, and current and future strategies to
1713 optimize efficacy.” *Journal of Affective Disorders* 88. Elsevier: 255–67.
- 1714 Lopes da Silva, Fernando. 2013. “EEG and MEG: relevance to neuroscience.” *Neuron* 80 (5).
1715 Elsevier Inc.: 1112–28. <https://doi.org/10.1016/j.neuron.2013.10.017>.
- 1716 Lubenov, E V, and A G Siapas. 2008. “Decoupling Through Synchrony in Neuronal Circuits
1717 with Propagation Delays.” *Neuron* 58: 118–31.
- 1718 Luke, T B, E Barreto, and P So. 2013. “Complete Classification of the Macroscopic Behaviour
1719 of a Heterogeneous Network of Theta Neurons.” *Neural Computation* 25: 3207–34.
- 1720 Lundqvist, M, J Rose, P Herman, S L Brincat, T J Buschman, and E K Miller. 2016. “Gamma
1721 and Beta Bursts Underlie Working Memory.” *Neuron* 90: 152–64.
- 1722 Martinet, L-E, G Fiddymont, J R Madsen, E N Eskandar, W Truccolo, U T Eden, SS Cash, and
1723 M A Kramer. n.d. “Human Seizures Couple Across Spatial Scales Through Travelling Wave
1724 Dynamics.” *Nature Communications* 8. The Author(s) SN -: 14896.
1725 <https://doi.org/10.1038/ncomms14896>.
- 1726 Mayberg, Helen S. 1997. “Limbic-Cortical Dysregulation: A Proposed Model of Depression.”
1727 *The Journal of Neuropsychiatry and Clinical Neurosciences* 9. American Psychiatric Assn:
1728 471–81.
- 1729 Meijer, H G E, T L Eissa, B Kiewiet, J F Neuman, C A Schevon, R G Emerson, R R Goodman, et
1730 al. 2015. “Modeling Focal Epileptic Activity in the Wilson–Cowan Model with

- 1731 Depolarization Block." *The Journal of Mathematical Neuroscience* 5: 7.
1732 <https://doi.org/10.1186/s13408-015-0019-4>.
- 1733 Menon, Vinod. 2011. "Large-Scale Brain Networks and Psychopathology: A Unifying Triple
1734 Network Model." *Trends in Cognitive Sciences* 15 (10). Elsevier: 483–506.
- 1735 Menon, Vinod, and Lucina Q Uddin. 2010. "Saliency, Switching, Attention and Control: A
1736 Network Model of Insula Function." *Brain Structure and Function* 214 (5-6). Springer: 655–
1737 67.
- 1738 Mi, Y, X Lin, and S Wu. 2016. "Neural Computations in a Dynamical System with Multiple
1739 Time Scales." *Frontiers in Computational Neuroscience* 10: 96.
- 1740 Montbrió, E, D Pazó, and A Roxin. 2015. "Macroscopic Description for Networks of Spiking
1741 Neurons." *Physical Review X* 5: 021028.
- 1742 Mormann, Florian, Klaus Lehnertz, Peter David, and Christian E Elger. 2000. "Mean Phase
1743 Coherence as a Measure for Phase Synchronization and Its Application to the EEG of
1744 Epilepsy Patients." *Physica D* 144 (3-4). Elsevier: 358–69.
- 1745 Mountcastle, V B. 1997. "The Columnar Organization of the Neocortex." *Brain* 120: 701–22.
- 1746 Muller, L, F Chavane, J Reynolds, and T J Sejnowski. 2018. "Cortical Travelling Waves:
1747 Mechanisms and Computational Principles." *Nature Reviews Neuroscience* 19: 255–68.
- 1748 Newman, M E J. 2016. "Mathematics of Networks." In *The New Palgrave Dictionary of
1749 Economics*, 1–8. London: Palgrave Macmillan UK.
- 1750 Noda, Y, W K Silverstein, M S Barr, F Vila-Rodriguez, J Downar, T K Rajji, P B Fitzgerald, et
1751 al. 2015. "Neurobiological Mechanisms of Repetitive Transcranial Magnetic Stimulation of
1752 the Dorsolateral Prefrontal Cortex in Depression: A Systematic Review." *Psychological
1753 Medicine* 45: 3411–32.
- 1754 Nunez, P L. 1974. "The Brain Wave Equation: A Model for the EEG." *Mathematical
1755 Biosciences* 21: 279–97.
- 1756 Nunez, P l. 1995. *Neocortical Dynamics and Human EEG Rhythms*. Edited by w. Oxford
1757 University Press.
- 1758 Onslow, A C E, M W Jones, and R Bogacz. 2014. "A Canonical Circuit for Generating Phase-
1759 Amplitude Coupling." *PLoS ONE* 9. Public Library of Science: 1–15.
1760 <https://doi.org/10.1371/journal.pone.0102591>.
- 1761 Park, Hae-Jeong, and Karl Friston. 2013. "Structural and Functional Brain Networks: From
1762 Connections to Cognition." *Science* 342 (6158). American Association for the Advancement
1763 of Science: 1238411.
- 1764 Pasley, Brian N, Elena A Allen, and Ralph D Freeman. 2009. "State-Dependent Variability of
1765 Neuronal Responses to Transcranial Magnetic Stimulation of the Visual Cortex." *Neuron* 62
1766 (2). Elsevier: 291–303.

- 1767 Peraza, Luis R., Ruth Cromarty, Xenia Kobeleva, Michael J. Firbank, Alison Killen, Sara
1768 Graziadio, Alan J. Thomas, John T. O'Brien, and John-Paul Taylor. 2018.
1769 "Electroencephalographic derived network differences in Lewy body dementia compared
1770 to Alzheimer's disease patients." *Scientific Reports* 8 (1): 4637.
- 1771 Pfurtscheller, G. 1999. "EEG Event-Related Desynchronization (ERD) and Event-Related
1772 Synchronization (ERS)." In *Electroencephalography. Basic Principles, Clinical Applications,*
1773 and *Related Fields*, edited by E Niedermeyer and F H Lopez da Silva, 4th ed., 958–67.
1774 Baltimore: Lippincott Williams; Wilkins.
- 1775 Pyle, R, and R Rosenbaum. 2017. "Spatiotemporal Dynamics and Reliable Computations in
1776 Recurrent Spiking Neural Networks." *Physical Review Letters* 118: 018103.
- 1777 Roberts, J A, L L Gollo, R G Abeysuriya, G Roberts, P B Mitchell, M W Woolrich, and M
1778 Breakspear. 2019. "Metastable Brain Waves." *Nature Communications* 10 (1056): 1–17.
- 1779 Robinson, P A. 2011. "Neural Field Theory of Synaptic Plasticity." *Journal of Theoretical*
1780 *Biology* 285: 156–63.
- 1781 Robson, Siân E., Matthew J. Brookes, Emma L. Hall, Lena Palaniyappan, Jyothika Kumar,
1782 Michael Skelton, Nikolaos G. Christodoulou, et al. 2016. "Abnormal visuomotor processing
1783 in schizophrenia." *NeuroImage: Clinical* 12: 869–78.
1784 <https://doi.org/10.1016/j.nicl.2015.08.005>.
- 1785 Rosenbaum, R, and B Doiron. 2014. "Balanced Networks of Spiking Neurons with Spatially
1786 Dependent Recurrent Connections." *Physical Review X* 4: 021039.
- 1787 Rothkegel, H, M Sommer, W Paulus, and N Lang. 2010. "Impact of Pulse Duration in Single
1788 Pulse Tms." *Clinical Neurophysiology* 121 (11). Elsevier: 1915–21.
- 1789 Rubinov, Mikail, Olaf Sporns, Cees van Leeuwen, and Michael Breakspear. 2009. "Symbiotic
1790 Relationship Between Brain Structure and Dynamics." *BMC Neuroscience* 10 (1). BioMed
1791 Central: 55.
- 1792 Rubinov, M, and O Sporns. 2010. "Complex network measures of brain connectivity: Uses
1793 and interpretations." *NeuroImage* 52: 1059–69.
- 1794 Rusu, Cătălin V, Max Murakami, Ulf Ziemann, and Jochen Triesch. 2014. "A model of TMS-
1795 induced I-waves in motor cortex." *Brain Stimulation* 7. Elsevier: 401–14.
- 1796 Sanz-Leon, P, S A Knock, A Spiegler, and V K Jirsa. 2015. "Mathematical Framework for
1797 Large-Scale Brain Network Modeling in the Virtual Brain." *NeuroImage* 111: 385–430.
- 1798 Schevon, Catherine A., Shennan A. Weiss, Guy McKhann Jr, Robert R. Goodman, Rafael
1799 Yuste, Ronald G. Emerson, and Andrew J. Trevelyan. n.d. "Evidence of an Inhibitory
1800 Restraint of Seizure Activity in Humans." *Nature Communications* 3. The Author(s) SN :-:
1801 1060. <https://doi.org/10.1038/ncomms2056>.

- 1802 Schulz, J B, L Hausmann, and J Hardy. 2016. "199 Years of Parkinson Disease – What Have
1803 We Learned and What Is the Path to the Future?" *Journal of Neurochemistry* 139: 3–7.
- 1804 Sherman, Maxwell A., Shane Lee, Robert Law, Saskia Haegens, Catherine A. Thorn, Matti S.
1805 Hämäläinen, Christopher I. Moore, and Stephanie R. Jones. 2016. "Neural Mechanisms of
1806 Transient Neocortical Beta Rhythms: Converging Evidence from Humans, Computational
1807 Modeling, Monkeys, and Mice." *Proceedings of the National Academy of Sciences* 113 (33).
1808 National Academy of Sciences: E4885–E4894. <https://doi.org/10.1073/pnas.1604135113>.
- 1809 Shimamoto, Hotetsu, Hitoyuki Morimitsu, Shunsuke Sugita, Kimihiro Nakahara, and Minoru
1810 Shigemori. 1999. "Therapeutic Effect of Repetitive Transcranial Magnetic Stimulation in
1811 Parkinson's Disease." *Rinsho Shinkeigaku* 39: 1264–7.
- 1812 Shusterman, V, and W C Troy. 2008. "From Baseline to Epileptiform Activity: A Path to
1813 Synchronized Rhythmicity in Large-Scale Neural Networks." *Physical Review E* 77: 061911.
- 1814 Siebner, Hartwig R, Gesa Hartwigsen, Tanja Kassuba, and John C Rothwell. 2009. "How
1815 Does Transcranial Magnetic Stimulation Modify Neuronal Activity in the Brain?
1816 Implications for Studies of Cognition." *Cortex* 45. Elsevier: 1035–42.
- 1817 Sotropoulos, Stamatis N, Moisés Hernández-Fernández, An T Vu, Jesper L Andersson,
1818 Steen Moeller, Essa Yacoub, Christophe Lenglet, Kamil Ugurbil, Timothy EJ Behrens, and
1819 Saad Jbabdi. 2016. "Fusion in diffusion MRI for improved fibre orientation estimation: An
1820 application to the 3T and 7T data of the Human Connectome Project." *NeuroImage* 134.
1821 Elsevier: 396–409.
- 1822 Sridharan, Devarajan, Daniel J Levitin, and Vinod Menon. 2008. "A Critical Role for the Right
1823 Fronto-Insular Cortex in Switching Between Central-Executive and Default-Mode
1824 Networks." *Proceedings of the National Academy of Sciences* 105 (34). National Acad
1825 Sciences: 12569–74.
- 1826 Stam, CJ, ECW van Straaten, E Van Dellen, P Tewarie, G Gong, A Hillebrand, J Meier, and P
1827 Van Mieghem. 2016. "The Relation Between Structural and Functional Connectivity
1828 Patterns in Complex Brain Networks." *International Journal of Psychophysiology* 103.
1829 Elsevier: 149–60.
- 1830 Stancák, Andrej, and Gert Pfurtscheller. 1995. "Desynchronization and recovery of β
1831 rhythms during brisk and slow self-paced finger movements in man." *Neuroscience Letters*
1832 196 (1-2). Elsevier: 21–24. [https://doi.org/10.1016/0304-3940\(95\)11827-J](https://doi.org/10.1016/0304-3940(95)11827-J).
- 1833 Straaten, Elisabeth CW van, and Cornelis J Stam. 2013. "Structure Out of Chaos: Functional
1834 Brain Network Analysis with EEG, MEG, and Functional MRI." *European
1835 Neuropsychopharmacology* 23 (1). Elsevier: 7–18.
- 1836 Tewarie, P, B A E Hunt, G C O'Neill, Á Byrne, K Aquino, M Bauer, K J Mullinger, S Coombes,
1837 and M J Brookes. 2018. "Relationships Between Neuronal Oscillatory Amplitude and
1838 Dynamic Functional Connectivity." *Cerebral Cortex* 29. Oxford University Press: 2668–81.

- 1839 Thomas Yeo, BT, Fenna M Krienen, Jorge Sepulcre, Mert R Sabuncu, Danial Lashkari, Marisa
1840 Hollinshead, Joshua L Roffman, et al. 2011. "The Organization of the Human Cerebral Cortex
1841 Estimated by Intrinsic Functional Connectivity." *Journal of Neurophysiology* 106. American
1842 Physiological Society Bethesda, MD: 1125–65.
- 1843 Tik, Martin, André Hoffmann, Ronald Sladky, Livia Tomova, Allan Hummer, Lucia Navarro
1844 de Lara, Henryk Bukowski, et al. 2017. "Towards understanding rTMS mechanism of
1845 action: stimulation of the DLPFC causes network-specific increase in functional
1846 connectivity." *NeuroImage* 162. Elsevier: 289–96.
- 1847 Touboul, Jonathan, Fabrice Wendling, Patrick Chauvel, and Olivier Faugeras. 2011. "Neural
1848 mass activity, bifurcations, and epilepsy." *Neural Computation* 23: 3232–86.
1849 https://doi.org/10.1162/NECO_a_00206.
- 1850 Valdes-Sosa, P A, J M Sanchez-Bornot, R C Sotero, Y Iturria-Medina, Y Aleman-Gomez, J
1851 Bosch-Bayard, F Carbonell, and T Ozaki. 2009. "Model driven EEG/fMRI fusion of brain
1852 oscillations." *Human Brain Mapping* 30: 2701–21.
- 1853 Van Den Heuvel, Martijn P, and Hilleke E Hulshoff Pol. 2010. "Exploring the Brain Network:
1854 A Review on Resting-State fMRI Functional Connectivity." *European
1855 Neuropsychopharmacology* 20 (8). Elsevier: 519–34.
- 1856 Van Essen, David C, Stephen M Smith, Deanna M Barch, Timothy EJ Behrens, Essa Yacoub,
1857 Kamil Ugurbil, Wu-Minn HCP Consortium, and others. 2013. "The WU-Minn human
1858 connectome project: an overview." *NeuroImage* 80. Elsevier: 62–79.
- 1859 Velazquez, J L Perez, and P L Carlen. 2000. "Gap Junctions, Synchrony and Seizures." *Trends
1860 in Neurosciences* 23: 68–74.
- 1861 Visser, S, R Nicks, O Faugeras, and S Coombes. 2017. "Standing and Travelling Waves in a
1862 Spherical Brain Model: The Nunez Model Revisited." *Physica D* 349: 27–45.
- 1863 Vogels, T P, H Sprekeler, F Zenke, C Clopath, and W Gerstner. 2011. "Inhibitory Plasticity
1864 Balances Excitation and Inhibition in Sensory Pathways and Memory Networks." *Science*
1865 334: 1569–73.
- 1866 Wang, X-J, and H Kennedy. 2016. "Brain Structure and Dynamics Across Scales: In Search of
1867 Rules." *Current Opinion in Neurobiology* 37: 92–98.
- 1868 Wendling, F, F. Bartolomei, J.J. Bellanger, and P. Chauvel. 2001. "Interpretation of
1869 interdependencies in epileptic signals using a macroscopic physiological model of the EEG."
1870 *Clinical Neurophysiology* 112 (7). Elsevier: 1201–18. [https://doi.org/10.1016/S1388-
1871 2457\(01\)00547-8](https://doi.org/10.1016/S1388-2457(01)00547-8).
- 1872 Wilson, H R, R Blake, and S-H Lee. 2001. "Dynamics of Travelling Waves in Visual
1873 Perception." *Nature* 412: 907–10.
- 1874 Wilson, H R, and J D Cowan. 1972. "Excitatory and Inhibitory Interactions in Localized
1875 Populations of Model Neurons." *Biophysical Journal* 12: 1–24.

- 1876 Wilson, H R, and J D Cowan. 1973. "A mathematical theory of the functional dynamics of
 1877 cortical and thalamic nervous tissue." *Biological Cybernetics* 13: 55–80.
- 1878 Wu, Jian-Young, Xiaoying Huang, and Chuan Zhang. 2008. "Propagating Waves of Activity in
 1879 the Neocortex: What They Are, What They Do." *The Neuroscientist* 14: 487–502.
- 1880 Xia M, Wang J, He Y. Brainnet viewer: a network visualization tool for human brain
 1881 connectomics. *PloS ONE* 8: e68910, 2013.
- 1882 Zetterberg, L H, L Kristiansson, and K Mossberg. 1978. "Performance of a Model for a Local
 1883 Neuron Population." *Biological Cybernetics* 31: 15–26.
- 1884 Zucker, R S, and W G Regehr. 2002. "Short-Term Synaptic Plasticity." *Annual Review of
 1885 Physiology* 64: 355–405.
- 1886

1887 **Figure captions**

- 1900 **Figure 1. Validation of mean field reduction.** Comparison of dynamics for mean field
 1901 f24386191 \h * MERGEFORMAT $Qg = \kappa f(Z)$,
 1902 $\frac{d}{dt}Z = FZ; \eta_0, \Delta + GZ, g; v_{syn}$, (4) and simulation of 500 coupled
 2023 $\frac{d}{dt}v_i = \eta_i + v_i^2 + g v_{syn} - v_i$, $Qg = \kappa N j = 1 N m \in Z \delta t - T_{jm}$, (7). (a) Phase plane of the
 2024 Kuramoto order parameter $Z = Re^{i\Psi}$. (b) Synaptic conductance g vs rate of change of
 2025 synaptic conductance g' . Parameter values: $\eta_0 = 20$, $\Delta = 0.5$, $v_{syn} = -10$, $\kappa = 1$, $\alpha = 0.95$
 2026
- 2027 **Figure 2. Beta rebound.** (a) Time frequency spectrogram showing percentage change
 2028 from baseline of a trial averaged signal from the motor cortex during a motor task. We see
 2029 stereotypical movement related beta decrease (MRBD) from 0–2 s and the post movement
 2030 beta rebound (PMBR) at roughly 2.5 s. (b) Time frequency spectrograms for schizophrenia
 2031 patients doing the same task. There is a significant decrease in PMBR. (c) Model results for
 2032 the Kuramoto order parameter during a simulated movement. Synchrony is maximal along
 2033 the dashed circle and minimal at the centre of the disk. The red curve shows the behaviour
 2034 during the simulated movement, while the green corresponds to the time after movement
 2035 termination. After movement termination there is an increase in synchrony (curve
 2036 approaches dashed line), before the system returns to its original behaviour. (d) Time
 2037 frequency spectrogram for the synaptic current, showing qualitatively similar properties to
 2038 the experimental results in (a). There is a reduction in beta power at movement onset (0 s),
 2039 followed by a sharp increase in power shortly after movement termination (0.5 s).
 2040 Parameter values: $\eta_0 = 21.5$, $\Delta = 0.5$, $v_{syn} = -10$, $\kappa = 0.105$, $\alpha^{-1} = 35\text{ms}$, $\tau = 31\text{ms}$. Data
 2041 for panel (a) and (b) from (Robson *et al.* 2015).

- 2042
- 2043 **Figure 3. Two hemisphere model.** Response of the system to a temporally filtered square
 2044 pulse of length 0.4 s and magnitude 10 μA . As in experimental findings, the contralateral
 2045 hemisphere shows a larger rebound than the ipsilateral hemisphere. Different initial
 2046 conditions were used for each row, resulting in different magnitudes and lengths of the

2047 rebound in oscillatory amplitudes. Parameter values: $\eta_0 = 23$, $\Delta = 0.5$, $v_{\text{syn}}^{ii} = -10$, $v_{\text{syn}}^{ij} =$
 2048 10 , $\kappa_{ii} = 4.5$, $\kappa_{ij} = 5.4$, $\alpha_{ii}^{-1} = 30$ ms, $\alpha_{ij}^{-1} = 75$ ms, $\tau = 30$ ms, were we use ii to denote
 2049 intra-hemisphere connections and ij for inter-hemisphere connections.

2050

2051 **Figure 4. Beta burst.** (a) Beta burst in single trial data, (2.5 s simulation). There is a peak
 2052 in beta-band power at roughly 800 ms, lasting ~ 200 ms. (b) Steady beta-band activity in
 2053 trial averaged data (average spectral power over 20 1 s simulations). Parameter values:
 2054 $\eta_0^E = 1.6$, $\eta_0^I = 1$, $\Delta_E = 0.2$, $\Delta_I = 0.2$, $v_{\text{syn}}^E = 10$, $v_{\text{syn}}^I = -12$, $\kappa_{EE} = 1$, $\kappa_{IE} = 1.5$, $\kappa_{EI} = 2$,
 2055 $\kappa_{II} = 1$, $\alpha_{EE}^{-1} = 3$ ms, $\alpha_{EI}^{-1} = 3$ ms, $\alpha_{IE}^{-1} = 10$ ms, $\alpha_{II}^{-1} = 10$ ms, $\tau_E = 12$ ms, $\tau_I = 18$ ms.

2056

2057 **Figure 5. Healthy versus epileptic oscillations.** For a large window in parameter space
 2058 the E-I population model (8) is multi-stable, different initial conditions can lead to different
 2059 behaviours, and small perturbations can also lead to a change in behaviour. (a) Regular
 2060 “health” oscillations. (b) Pathological seizure-like oscillations. (c) A small perturbation to
 2061 the E-E synaptic conductance gives rise to a transition from healthy to pathological
 2062 behaviour. Parameter values: $\eta_0^E = 10$, $\eta_0^I = 21$, $\Delta_E = 0.5$, $\Delta_I = 0.5$, $v_{\text{syn}}^E = 10$, $v_{\text{syn}}^I = -10$,
 2063 $\kappa_{EE} = 1.5$, $\kappa_{IE} = 1.5$, $\kappa_{EI} = 4.5$, $\kappa_{II} = 2.4$, $\alpha_{EE}^{-1} = 6.5$ ms, $\alpha_{EI}^{-1} = 20$ ms, $\alpha_{IE}^{-1} = 5$ ms, $\alpha_{II}^{-1} = 7$
 2064 ms, $\tau_E = 3$ ms, $\tau_I = 3$ ms.

2065

2066 **Figure 6.** Visual representation of (a) structural network and (b) simulated functional
 2067 network. The surface of the brain visualisations are coloured depending on nodal degree,
 2068 which was normalised by the highest element for easier comparison between SC and FC.
 2069 The network graphs are shown on the bottom row. Parameter values: $\alpha_{EE}^{mn} = 1$, $\alpha_{IE}^{mn} = 1.4$,
 2070 $\alpha_{EI}^{mn} = 0.7$, $\alpha_{II}^{mn} = 0.4$, $\kappa_{EE}^{mn} = 1.5$, $\kappa_{IE}^{mn} = 1$, $\kappa_{EI}^{mn} = 2$, $\kappa_{II}^{mn} = 3$, $v_{EE} = 10$, $v_{mn}^{IE} = 8$, $v_{mn}^{EI} = -8$,
 2071 $v_{\text{syn},mn}^{II} = -12$, $\Delta_m^E = 0.5$, $\Delta_m^I = 0.5$, $n_{0,m}^I = -20$, $n_{0,m}^E = 20$, $\tau_m^a = 1$; values of κ_{EE}^{mn} are
 2072 obtained from MRI data (see text), scaled by a global coupling strength $\varepsilon = 0.025$.

2073

2074 **Figure 7.** Normalised node degree of FC networks under rTMS stimulation of each cortical
 2075 area. FC matrices are interpolated on brain meshes of the right hemisphere. The node
 2076 representing the right anterior insula is also shown to depict the relative influence on
 2077 stimulation of nodes on a specific sub-cortical region. Figures created with BrainNet
 2078 Viewer (Xia *et al.*, 2013). Parameters as in Figure 6.

2079

2080 **Figure 8.** Graph properties of the right anterior insula in FC networks obtained under
 2081 rTMS stimulation of each cortical area. Shown is: the shortest path length between the
 2082 stimulated area and the right anterior insula; and the eigencentrality, clustering coefficient,
 2083 and node degree of the insula node. Parameters as in Figure 6.

2084

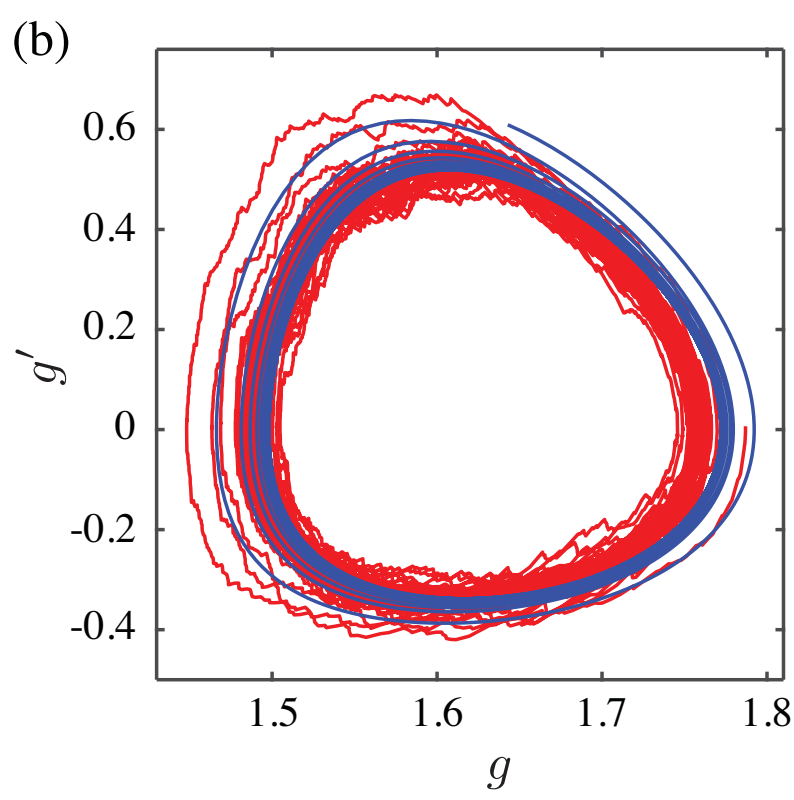
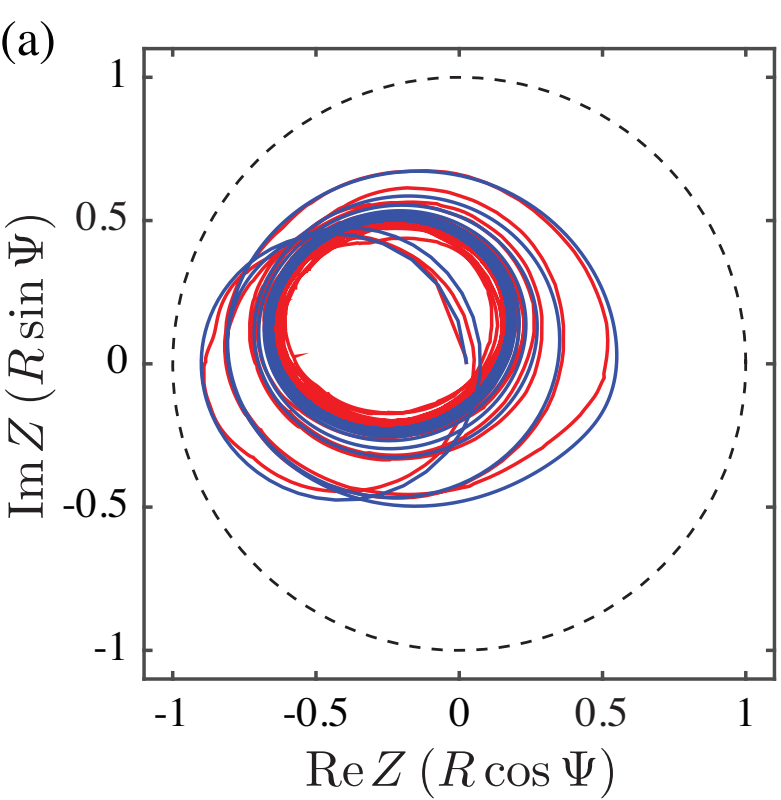
2085 **Figure 9.** The speed of a travelling pulse in a one dimensional spatial model. The main plot
 2086 shows the wave speed as a function of the axonal velocity v , highlighting that causality is
 2087 enforced so that $v < c$, as expected. The figure also highlights that for large v the wave-

2088 speed saturates. The insets show a spatial profile for $g = g(x, t)$ at some fixed time t .
2089 Encoded on top of this are the values of R and Ψ , where $Z = R e^{i\Psi}$, showing how the degree
2090 of synchrony R can vary quite rapidly within a pulse, whilst the phase Ψ switches from just
2091 greater than $-\pi$ outside a pulse to roughly π within a pulse. Parameter values: $v = 5$,
2092 $\sigma = 1$, $\eta_0 = -3$, $\Delta = 0.5$, $v_{\text{syn}} = 5$, $\kappa = 5$, $\tau_A = 30$, $\alpha = 1$, $\delta = 5$.

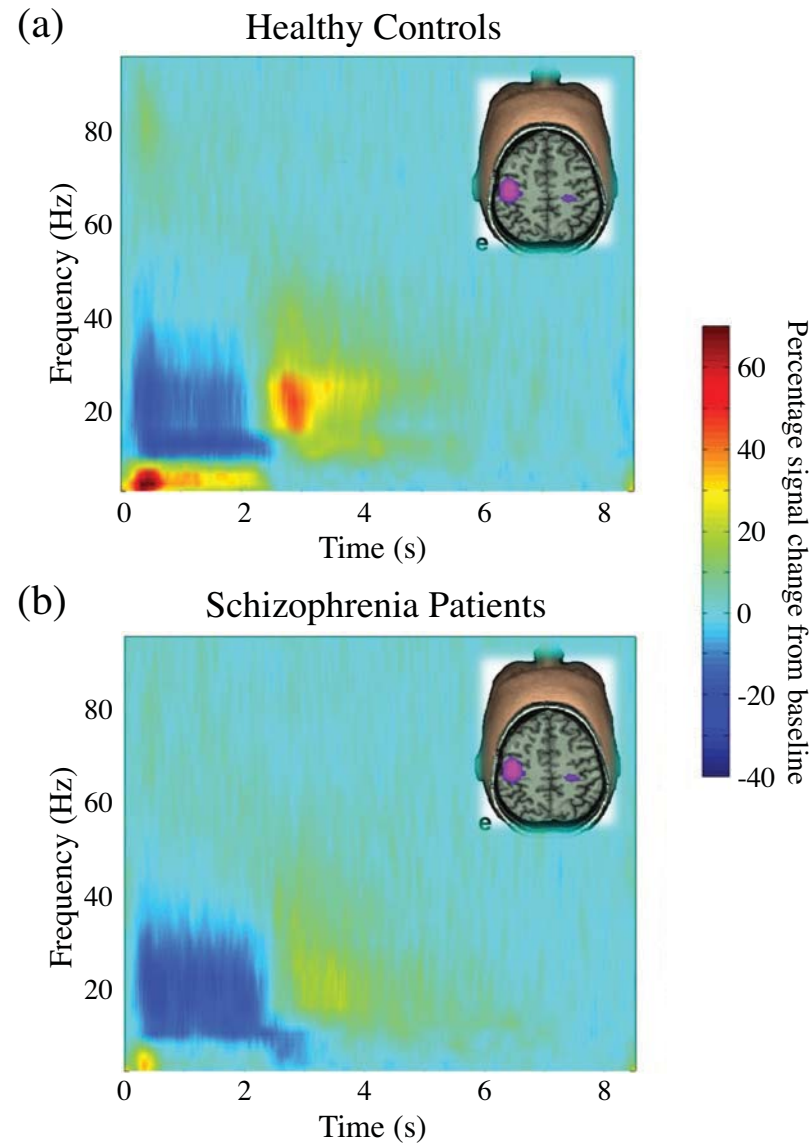
2093
2094

2095 **Figure 10.** The spread of a travelling ring in a two dimensional spatial model. The images
2096 show the magnitude of the synchrony order parameter $|Z| = R(\mathbf{r}, t)$ for different values of
2097 time t , with $\mathbf{r} = (\mathbf{x}, \mathbf{y})$. The wave is initiated with a localised spatial pulse input in the
2098 centre of a planar domain. Parameter values: $v = 10$, $\sigma = 1$, $\eta_0 = -3$, $\Delta = 0.5$, $v_{\text{syn}} = 5$,
2099 $\kappa = 5$, $\tau_A = 30$, $\alpha = 1$, $\delta = 15$.

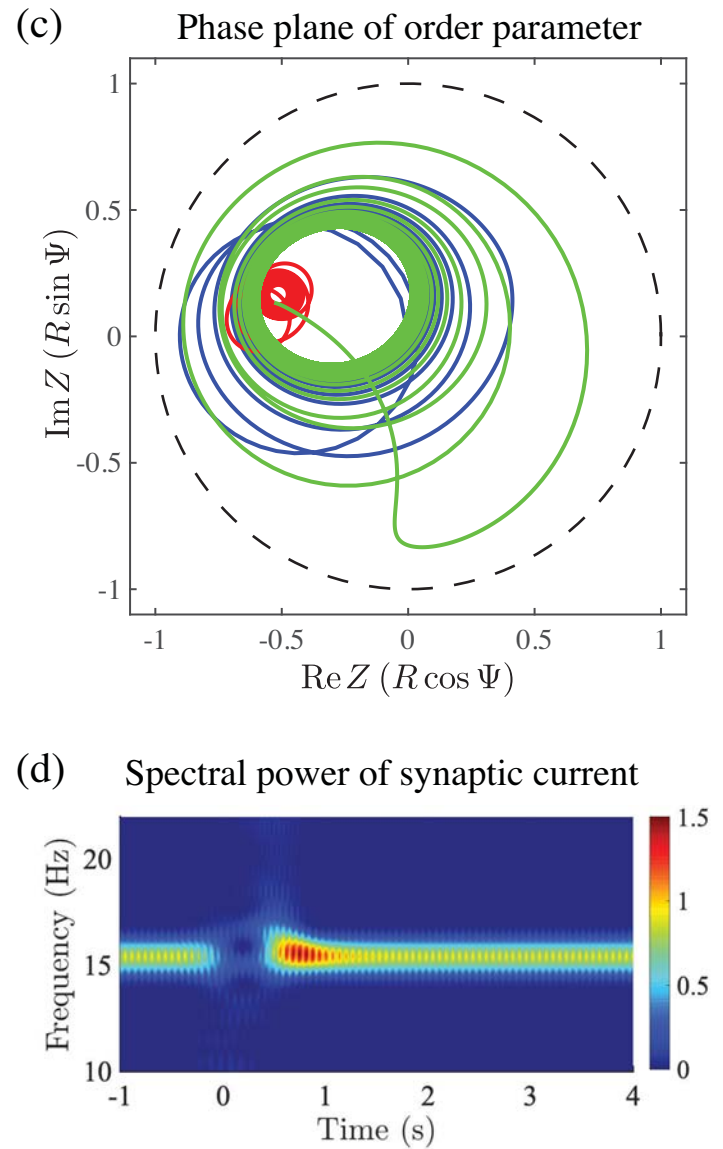
2100
2101

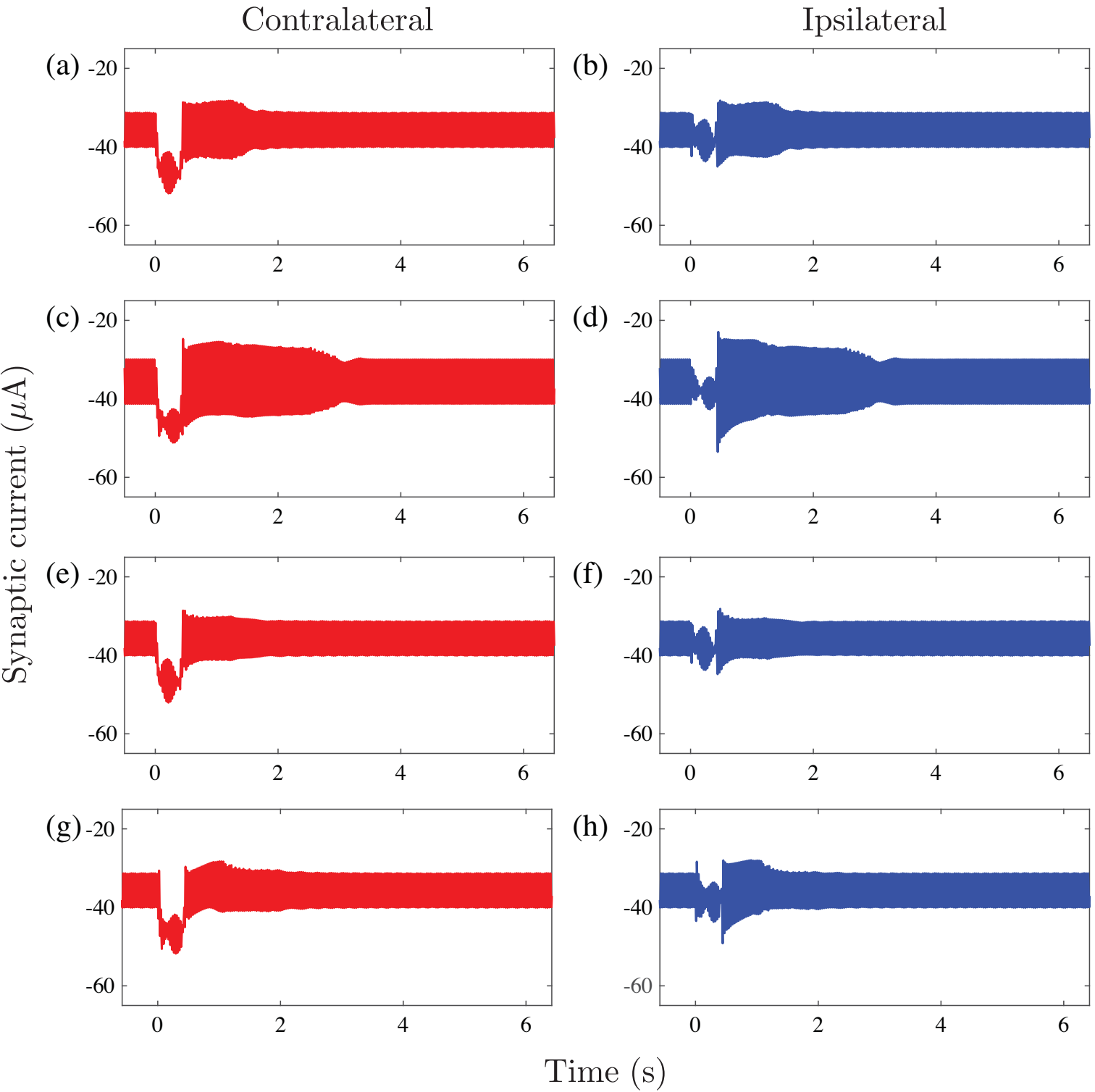


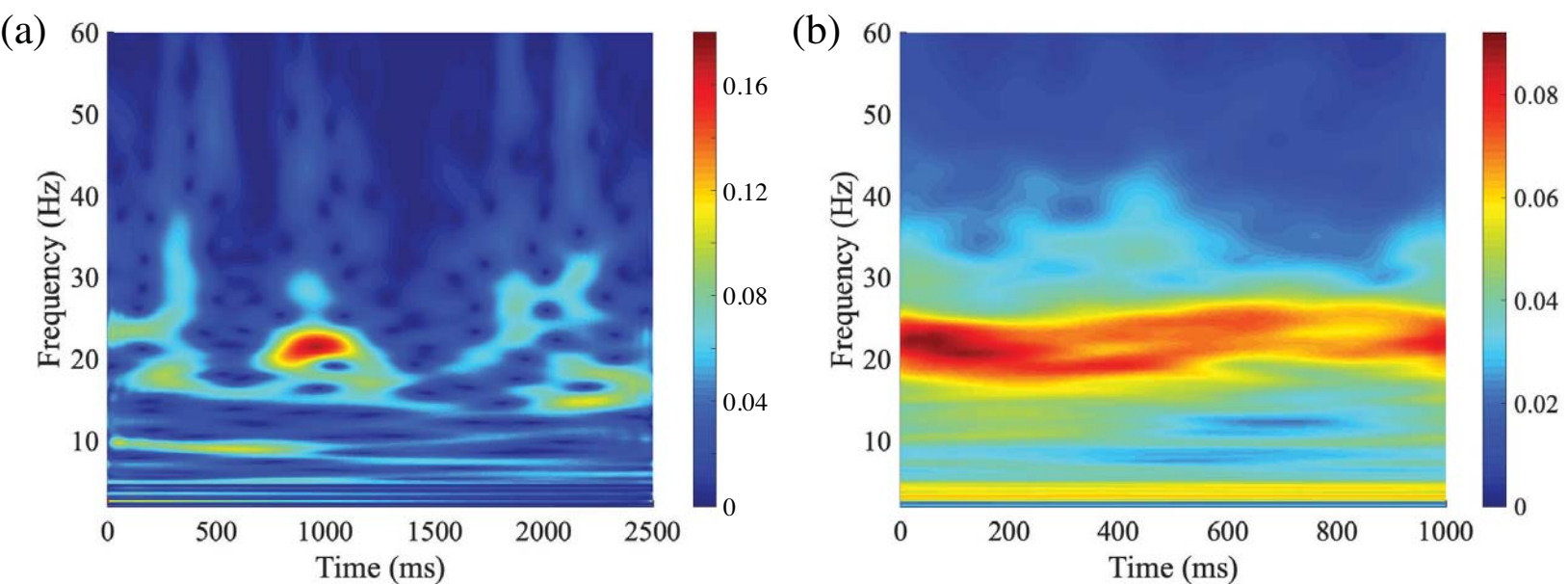
Experimental results

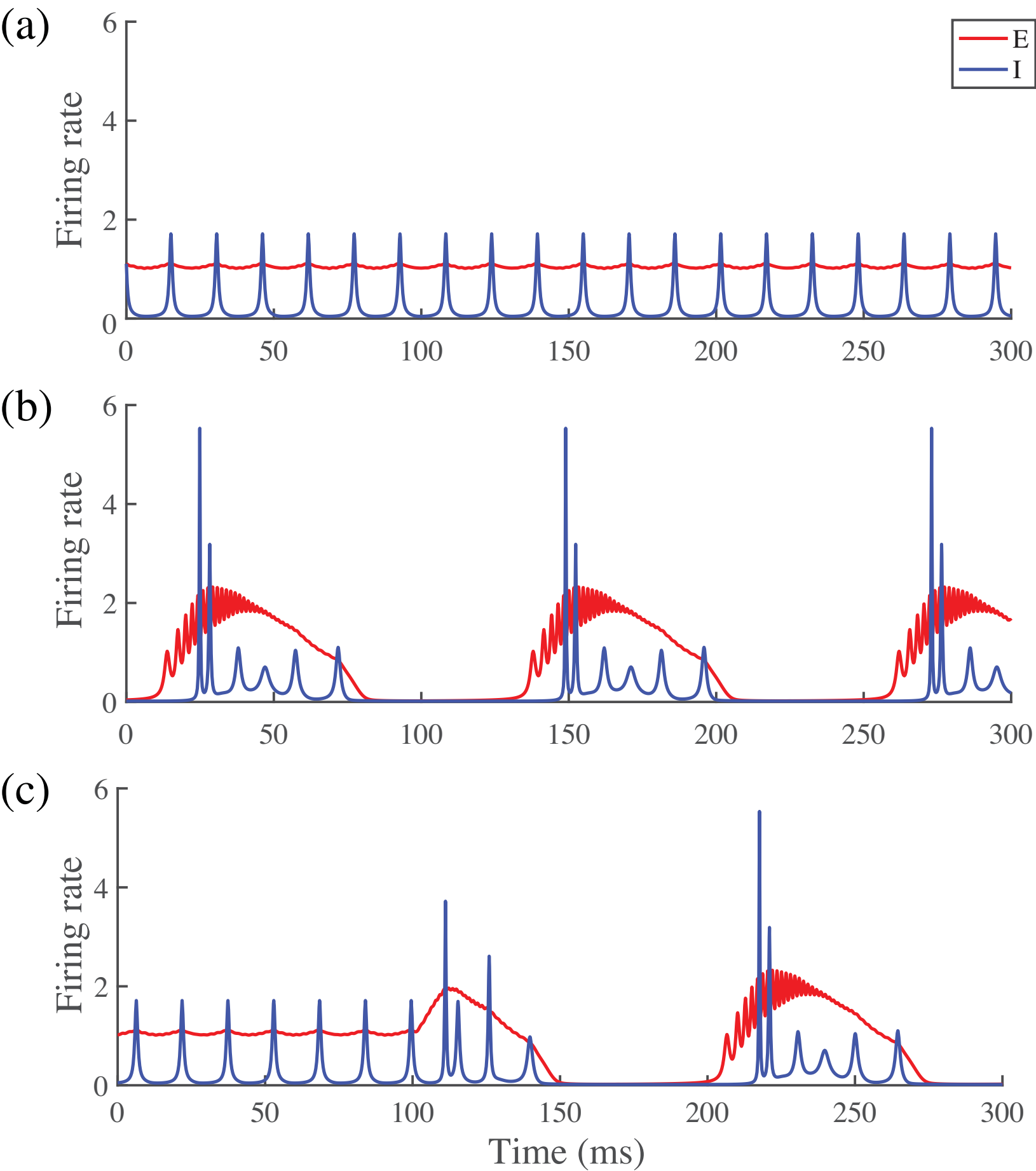


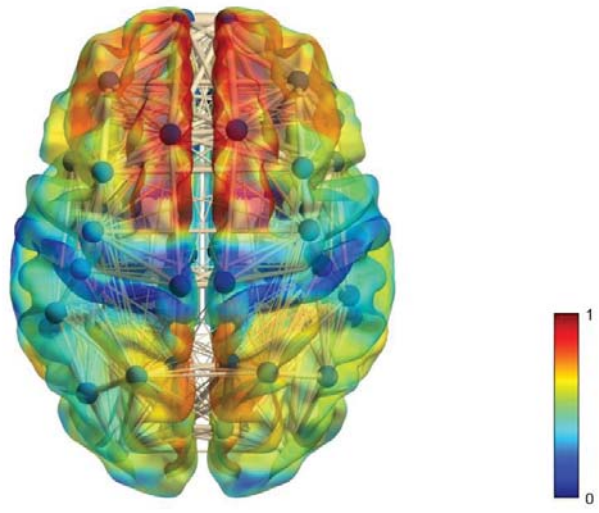
Model behaviour



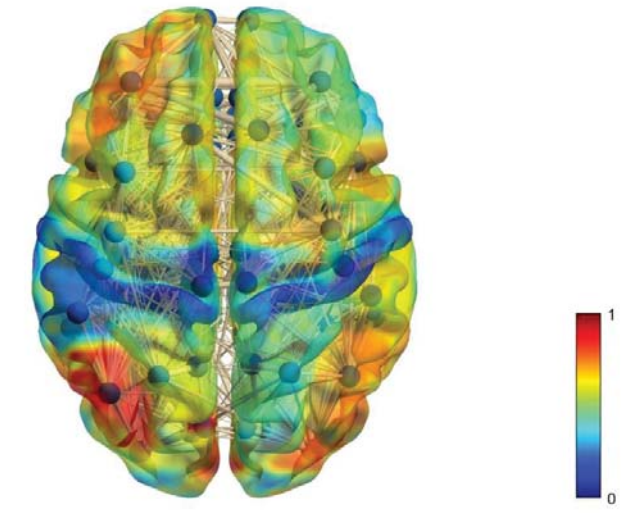
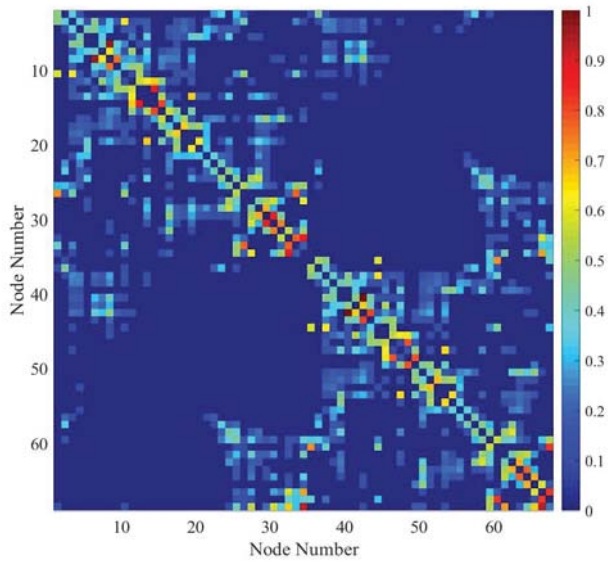




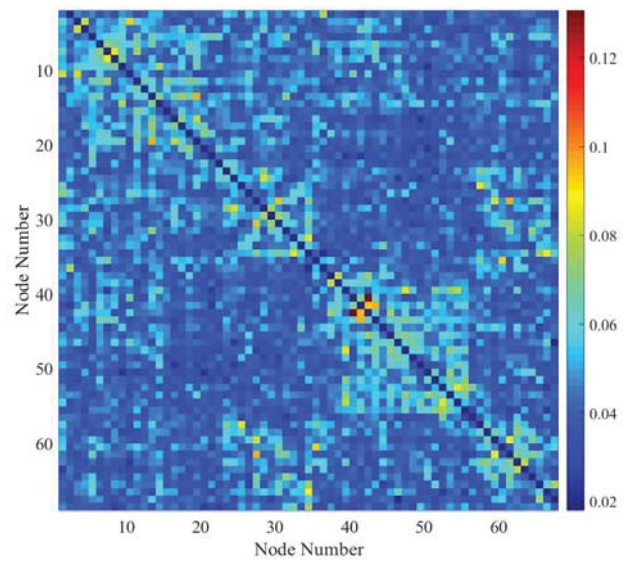


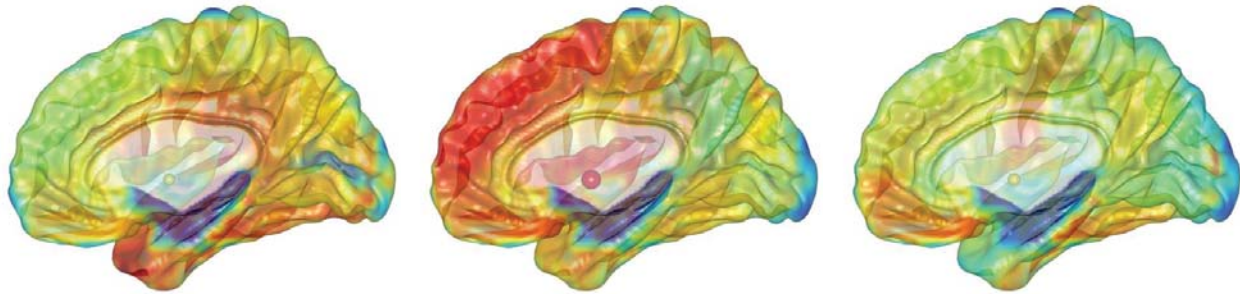


(a)



(b)

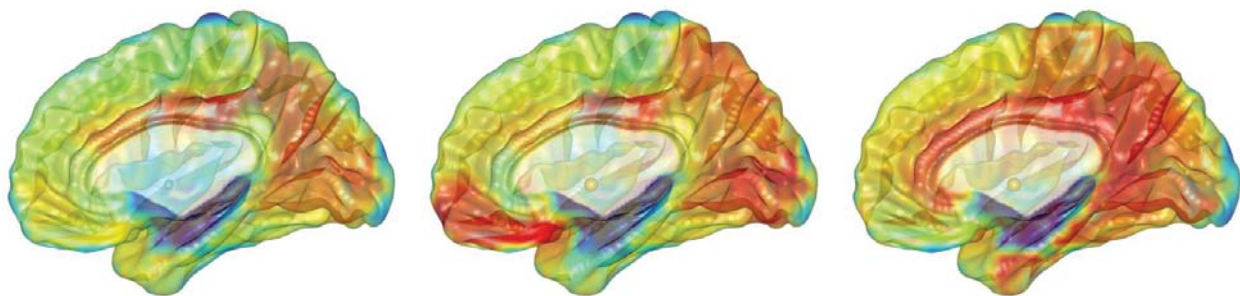




(a) No TMS
 $J=0.1070$

(b) L. Posterior cingulate
 $J=0.1556$

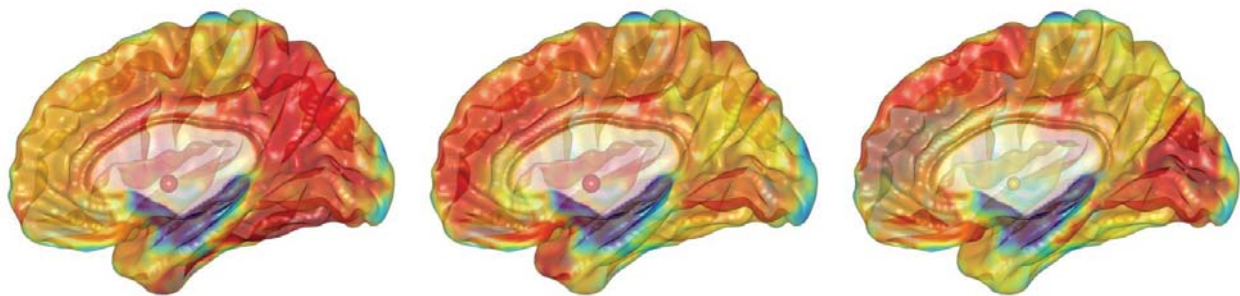
(c) L. Isthmus Cingulate
 $J=0.1414$



(d) L. Entorhinal
 $J=0.1328$

(e) L. Caudal anterior cingulate
 $J=0.1701$

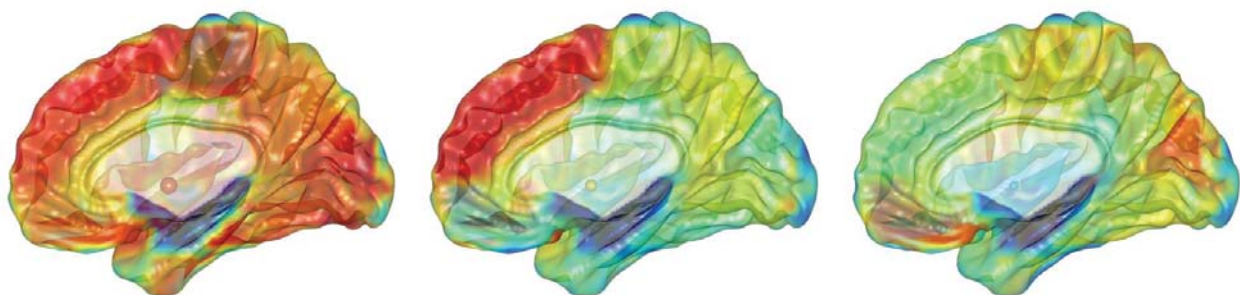
(f) L. Lateral orbitofrontal
 $J=0.1467$



(g) L. Medial orbitofrontal
 $J=0.1795$

(h) L. Rostral anterior cingulate
 $J=0.1646$

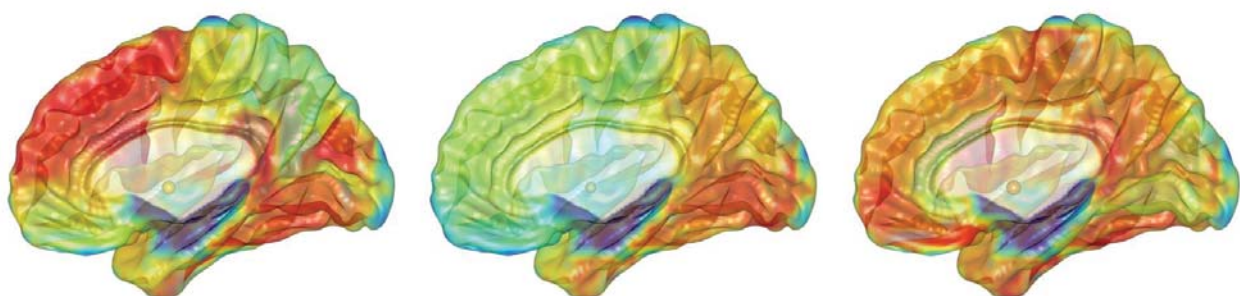
(i) R. Posterior cingulate
(ii) J=0.1418



(j) R. Isthmus Cingulate
 $J=0.1494$

(k) R. Entorhinal
 $J=0.1611$

(l) R. Caudal anterior cingulate
 $J=0.1443$



(m) R. Lateral orbitofrontal
 $J=0.1573$

(n) R. Medial orbitofrontal
 $J=0.1536$

(o) R. Rostral anterior cingulate
 $J=0.1448$

